

5-15-2018

Numerical Analysis of an Electrical Transformer with Fins and Horizontal Pins

Sean Ferneyhough
ferneyhough.sean@gmail.com

Follow this and additional works at: <https://digitalscholarship.unlv.edu/thesesdissertations>

 Part of the [Mechanical Engineering Commons](#)

Repository Citation

Ferneyhough, Sean, "Numerical Analysis of an Electrical Transformer with Fins and Horizontal Pins" (2018). *UNLV Theses, Dissertations, Professional Papers, and Capstones*. 3251.
<https://digitalscholarship.unlv.edu/thesesdissertations/3251>

This Thesis is protected by copyright and/or related rights. It has been brought to you by Digital Scholarship@UNLV with permission from the rights-holder(s). You are free to use this Thesis in any way that is permitted by the copyright and related rights legislation that applies to your use. For other uses you need to obtain permission from the rights-holder(s) directly, unless additional rights are indicated by a Creative Commons license in the record and/or on the work itself.

This Thesis has been accepted for inclusion in UNLV Theses, Dissertations, Professional Papers, and Capstones by an authorized administrator of Digital Scholarship@UNLV. For more information, please contact digitalscholarship@unlv.edu.

NUMERICAL ANALYSIS OF AN ELECTRICAL TRANSFORMER WITH FINS AND HORIZONTAL PINS

By

Sean Ferneyhough

Bachelor of Science- Mechanical Engineering

University of Nevada, Reno

2015

A thesis submitted in partial fulfillment

of the requirements for the

Master of Science in Engineering- Mechanical Engineering

Department of Mechanical Engineering

Howard R. Hughes College of Engineering

The Graduate College

University of Nevada, Las Vegas

May 2018



Thesis Approval

The Graduate College
The University of Nevada, Las Vegas

April 13, 2018

This thesis prepared by

Sean Ferneyhough

entitled

Numerical Analysis of an Electrical Transformer with Fins and Horizontal Pins

is approved in partial fulfillment of the requirements for the degree of

Master of Science in Engineering- Mechanical Engineering
Department of Mechanical Engineering

Samir Moujaes, Ph.D.
Examination Committee Chair

Kathryn Hausbeck Korgan, Ph.D.
Graduate College Interim Dean

Darrell Pepper, Ph.D.
Examination Committee Member

Hui Zhao, Ph.D.
Examination Committee Member

Saaman Ladkany, Ph.D.
Graduate College Faculty Representative

Abstract

Three-dimensional numerical simulations are run on a cylindrical electrical transformer that is generating heat in order to study the resulting natural convection that is driven by density variation. The transformer generates a constant heat flux and is incased in a sleeve with radial fins. At first, the sleeve is analyzed without fins and compared to an analytical solution in order to validate the numerical simulations. Next, fins are added to the sleeve in order to maximize the heat transfer from the transformer. Heat transfer from the sleeve per number of fins is to be determined.

Small pins are then added to the channels between the fins in order to perturb the flow and thermal boundary layer with the goal of increasing heat transfer. Results show that adding the pins to both the base and fins increases heat transfer but adding pins to the base alone does not guarantee an increase in heat transfer.

Table of Contents

Abstract.....	iii
Table of Contents.....	iv
List of Tables	v
List of Figures	vi
1. Introduction	1
2. Problem Statement.....	4
2.1 Analytical Solution	7
2.2 Comparison with Numerical Model.....	12
3. 3D Numerical Simulation Setup	17
3.1 Mesh Independence Parametric Studies	24
4. SolidWorks Flow Simulation	26
4.1 Mesh Generation	26
4.2 Flow Simulation Equations.....	26
4.3 Boundary Layer Treatment	31
4.4 Flow Simulation Adaptive Mesh	32
5. Results	36
5.1 Adaptive Mesh	36
5.2 Fluid Velocity.....	38
5.3 Transformer Temperature Comparison.....	50
5.4 Convective Heat Transfer Coefficient	59
Conclusion.....	67
References	69
Curriculum Vitae	71

List of Tables

Table 1: Temperature as a function of z (radius) for the finless sleeve from SolidWorks Simulation.....	15
Table 2: Maximum fluid velocities for each configuration.	49
Table 3: Maximum transformer temperature for each configuration	50
Table 4: ΔT for each configuration.....	50
Table 5: Convective heat transfer coefficient calculated for each configuration.	60

List of Figures

Figure 1: Default configuration- transformer with 30 fins without pins.	5
Figure 2: Configuration 1- transformer with 30 fins with pins on the base of the sleeve only.....	5
Figure 3: Configuration 2- transformer with 30 fins with pins on the base of the sleeve as well as the fins.	6
Figure 4: Simplified geometry used to solve an analytical solution that will be used to validate the numerical simulations.....	7
Figure 5: Material properties for Al 6061 from SolidWorks material library. Thermal conductivity will be used in the analytical solution.	7
Figure 6: Convection boundary condition on the finless sleeve. Note that $h=30 \text{ W/m}^2\text{-K}$ and the ambient temperature is 305 K.	13
Figure 7: Heat flux boundary condition on the inner sleeve surface. $q''=1687.5 \text{ W/m}^2$	13
Figure 8: Closeup of the mesh density that is used to calculate the temperature distribution in the finless sleeve. This mesh is dense enough that the temperature no longer changes with a change in mesh size.	14
Figure 9: Finless sleeve temperature distribution shown on the model geometry.	14
Figure 10: Analytical calculation of T for the values of r that correspond to the locations of the probe in table 1.	16
Figure 11: Graph of analytical vs numerical data for the finless sleeve shows that the simulation is indeed validated.	16
Figure 12: Simulation Wizard selections for analysis type. Gravity is in the y-direction.....	17
Figure 13: Initial conditions for the transformer in natural convection. Ambient temperature and pressure are chosen as 293.2 K and 101325 Pa- atmospheric conditions. Zero velocity parameters are defined to model still air that is only affected by the transformer heat.....	18

Figure 14: Default computational domain generated by the Flow Simulation package is far too large for a calculation with a dense mesh.....	19
Figure 15: Computational domain with simplifications. The shaded grey region is the actual volume that is used in calculations, and the dashed region represents the total volume that is reduced by the use of symmetry in the x and z-directions.....	20
Figure 16: Flow Simulation Analysis tree used to generate the appropriate conditions for the simulation. No fluid subdomains are defined since the entire fluid domain is assumed to be air.	20
Figure 17: Heat Generation Rate of 2500 W applied to the transformer volume.....	21
Figure 18: Goals selected for each of the simulation studies.	22
Figure 19: Local mesh defined by a rectangular prism that encompasses the entire transformer solid with adequate surrounding fluid volume. This region will be more greatly refined to improve calculation results.	23
Figure 20: Parametric study of the maximum fluid temperature as a function of number of cells.....	24
Figure 21: Parametric study of the maximum fluid velocity as a function of number of cells.....	24
Figure 22: Calculation Control Options dialogue box used to specify criteria for the adaptive mesh refinements.....	34
Figure 23: Adaptive mesh generated for the fluid region for the simple transformer with 40 fins and no pins.....	36
Figure 24: Close up of the mesh with the model geometry hidden. The orange and red sections show the increased mesh density at the fluid/solid boundary in the fin channels.....	37
Figure 25: Mesh generated on the solid transformer fins.....	37
Figure 26: Flow trajectory for the default transformer with 40 fins.	40
Figure 27: Isometric view of Fig. 28.	41
Figure 28: Flow trajectory for configuration 1 between 3 fins only.	42

Figure 29: Isometric view of the flow trajectories above.	43
Figure 30: Flow trajectory for configuration 2.	44
Figure 31: Isometric view of Fig. 30.	45
Figure 32: Cut plot showing the fluid velocity for the default configuration.	46
Figure 33: Cut plot showing the fluid velocity for configuration 2.	47
Figure 34: Close up of the fluid velocity at the top edge of the transformer for configuration 2.	48
Figure 35: Maximum fluid velocities graphed for each configuration.	49
Figure 36: Maximum transformer volume temperature graphed as a function of number of fins for the 3 geometries.	51
Figure 37: Isometric view of config. 1 shown with a cut plot of fluid temperature between the fins.	52
Figure 38: Cut plot of fluid temperature- default configuration.	54
Figure 39: Cut plot of fluid temperature- configuration 1.	54
Figure 40: Cut plot of fluid temperature- configuration 2.	54
Figure 41: Close up of Fig. 38.	55
Figure 42: Close up of Fig. 39.	55
Figure 43: Close up of Fig. 40.	55
Figure 44: Transformer surface temperature- default configuration.	56
Figure 45: Transformer surface temperature- configuration 1.	57
Figure 46: Transformer surface temperature- configuration 2.	58
Figure 47: Graphical representation of the convective heat transfer coefficient per # of fins.	60
Figure 48: Configuration 2 with 50 fins.	61
Figure 49: Configuration 2 with 60 fins.	62
Figure 50: Cut plot of fluid temperature for configuration 2 with 50 fins.	63
Figure 51: Cut plot of fluid temperature for configuration 2 with 60 fins.	64

Figure 52: Close up of the wake at the top edge of the transformer from Fig. 50..... 65

Figure 53: Close up of the wake at the top edge of the transformer from Fig. 51..... 66

1. Introduction

Heat augmentation with the use of fins has been studied extensively for many different applications. Fin shape, convection type, material selection, manufacturability, and fin array geometry are all factors that are considered to increase heat transfer. Pin and fin density on a heat sink was evaluated experimentally and found the optimal spacing, height, and cross-section for aluminum pins and fins in low velocity applications [1].

Small scale electrical devices rely on fin or topology optimization in order to maximize heat transfer while adhering to strict space requirements. Topology optimization was initially used in structural engineering to design members that minimize weight while maximizing strength. The same technique can be directly applied to conduction heat transfer problems to numerically generate optimized geometries that maximize heat transfer [2]. Finite element computational codes have been developed that use a material's thermal conductivity as the design variable. The temperature of the control region can then be reduced by adding or subtracting material from individual elements [3]. Codes to perform geometric topology optimization are available for numerous readily available software packages such as COMSOL and MATLAB [4-5].

Buoyancy forces developed by differences in fluid density are the driving forces in natural convection. Many studies have been conducted on optimizing fins in natural convection. Numerical schemes have been used to determine the optimal distance between vertical channels in natural convection, with the intent of applying the findings in small electronic packaging [6]. Temperature differences, plate separation distance, and plate length were also investigated numerically using a three-dimensional finite volume CFD code [7]. Experimental results have also been obtained for free convection between two horizontal plates as a function of the plate width [8], as well as heat transfer coefficient correlations for vertical and horizontal free surfaces in buildings [9]. Several numerical and experimental

studies have been conducted on adding obstructions to vertical channels in natural convection in order to disturb the thermal boundary layer and increase heat transfer [10-12].

Examinations of the development of thermal boundary layers have been a popular research topic over the last century. When fluid flow passes over a plate, both thermal and velocity boundary layers develop. In these regions, where either the velocity or the temperature is less than or equal to 99% of the free-stream values, heat transfer is reduced. This is an important phenomenon, and therefore numerous experimental and numerical studies have been done in order to develop relationships to express the length and thickness of the boundary layer. One such study experimentally examined the correlation between Rayleigh number and boundary layer thickness in both laminar and turbulent regimes [13]. Conclusions from these types of studies are to minimize the boundary layer thickness in order to maximize heat transfer. Disturbing the flow using obstructions is one method of minimizing boundary layer thickness.

Traditional methods of manufacturing heat sinks have been perfected over the years. Different categories of heat sinks require different manufacturing techniques. Such categories of heat sinks include passive heat sinks, which rely solely on natural convection for cooling, semi-active heat sinks which use fans that already exist in the system, active heat which rely on forced convection from a dedicated fan, liquid cooled devices that used circulated water or oils in order to cool the array, or phase change devices that use boilers and condensers to dissipate heat [14]. Creating the pin arrays for these categories employ several different methods. Firstly, stamping conductive metals like copper and aluminum into the desired shape is a low-cost technique and also can produce high volumes, but cannot handle large temperature differences. Extruding and machining fins is another option that can produce intricate 2D shapes that can be used in high heat gradients. Drawbacks on this method include high costs of manufacturing and low output capacity. Bonding fins to base plates using highly conductive epoxy increases the surface area of heat sinks in order to take advantage of convective heat transfer. Pins and fins can also be cast using sand

dies in order to produce high density arrays at an increased manufacturing cost. Lastly, folding sheet metal into fins can be accomplished, at the detriment of fin efficiency.

Manufacturing techniques have been improving drastically over the past decades due to technological advances. Before, only simple pin and fin designs could be used in order to increase heat transfer since complex shapes were either impossible to create or were simply too cost prohibitive to justify the improvements. 3D printing advancements have started to make manufacturing the complex shapes produced by topology optimization a reality. When it comes to producing these shapes for metal fins, additive layer manufacturing, or ALM, is the method of choice. Recent experiments have been conducted on fins that have manufactured using ALM to produce the optimized topology in order to maximize heat transfer in a given volume [15]. ALM can produce all the same shapes as the previously discussed techniques and requires little labor or production expertise. Another modern manufacturing technique is micro deformation technology, or MDT, which uses a fixed tool that passes over a section of material to deform the piece into pin and fin patterns [16]. Unlike machining or etching, MDT does not deplete material but rather just deforms the base material into the desired shape which saves money and resources.

In conclusion from the literature search, there is a lack of 3D numerical simulation data for large scale fins in natural convection that use horizontal fins in order to disturb the flow through the vertical channels. An investigation into whether adding these pins to the vertical channels will increase the heat transfer coefficient by disturbing the thermal boundary layer will tie several of the main topics together into one large scale CFD simulation. Due to the advances in manufacturing techniques, producing this pin and fin configuration will no longer be an issue.

2. Problem Statement

A 3D numerical simulation is conducted using SolidWorks Flow Simulation 2016 on a large cylindrical electrical transformer that is generating a constant heat density of 2500 W/m^3 and is being cooled by natural convection. The transformer is encased in a cylindrical sleeve that will incorporate fins in order to reduce the maximum temperature of the transformer volume. The number of fins on the sleeve will be ranged from 30-60 in an increment of 10 fins in order to observe the heat transfer coefficient as a function of number of fins. Next, small horizontal pins will be placed on the sleeve base with the goal of disturbing the flow and therefore decreasing the thermal boundary layer. Finally, the pins are extended to cover the height of the fins as well to further disrupt the flow and maximize heat transfer. Fin geometry and number are kept constant for the three simulations.

The transformer geometry is generated in SolidWorks and can be seen below in Fig. 1-3 for the three different configurations for the first test case of 30 fins. Transformer diameter is 2.7m, and the sleeve diameter is 3m. Length in the y-direction is 3m. The fins extend 0.25m from the sleeve and are 0.1m in thickness. The pins add an additional 0.01m in the radial direction to the sleeve and are equally spaced down the length of the transformer, with 6 pins in total per channel. Such a large geometry is used by design in order to study the flow up the channels that is produced by natural convection.

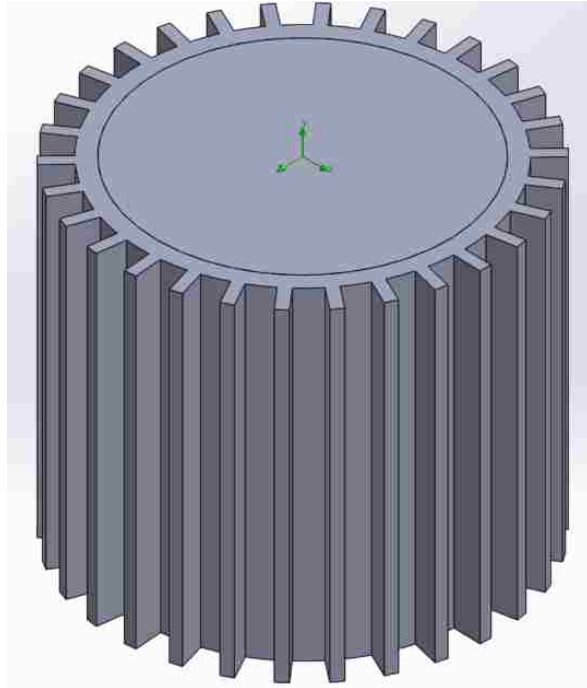


Figure 1: Default configuration- transformer with 30 fins without pins.

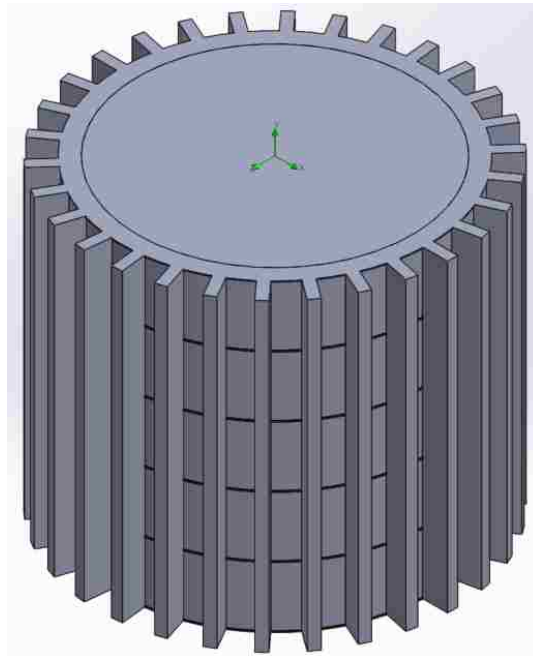


Figure 2: Configuration 1- transformer with 30 fins with pins on the base of the sleeve only.

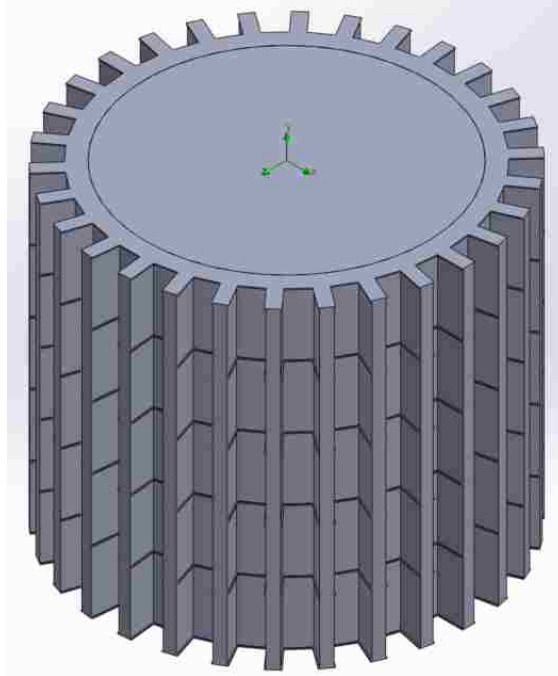


Figure 3: Configuration 2- transformer with 30 fins with pins on the base of the sleeve as well as the fins.

A 2D simplification is made in order to use an analytical solution to validate the numerical model. A 1m section cut is made from the top of the transformer in order to make the simplification; all heat transfer results will be on a per-unit length basis. Since analytical solutions require an easily define boundary, the sleeve is analyzed without fins or pins to create a cylindrical model. Figure 4 shows the greatly simplified geometry that will be analyzed analytically. The temperature profile through the sleeve will be determined using a constant convective heat transfer coefficient on the outside surface of 30 W/m^2-K . Ambient temperature is assumed to be a constant 305 K.

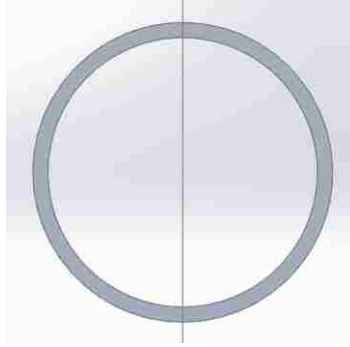


Figure 4: Simplified geometry used to solve an analytical solution that will be used to validate the numerical simulations.

The transformer and sleeve are both Al 6061, with material properties as defined in the SolidWorks library. Figure 5 below shows the properties as defined in SolidWorks.

Property	Value	Units
Elastic Modulus	6.9e+010	N/m ²
Poisson's Ratio	0.33	N/A
Shear Modulus	2.6e+010	N/m ²
Mass Density	2700	kg/m ³
Tensile Strength	124084000	N/m ²
Compressive Strength		N/m ²
Yield Strength	55148500	N/m ²
Thermal Expansion Coefficient	2.4e-005	/K
Thermal Conductivity	170	W/(m·K)

Figure 5: Material properties for Al 6061 from SolidWorks material library. Thermal conductivity will be used in the analytical solution.

2.1 Analytical Solution

With the simplifications made to the geometry as seen in Fig 2. and assuming the cylinder is long in the axial direction, the problem can be reduced to 1D and can be solved analytically. We begin with the 1D heat equation in cylindrical coordinates:

$$\frac{1}{r} \frac{\partial}{\partial r} \left[k_r r \frac{\partial T}{\partial r} \right] + q''' = \rho c \frac{\partial T}{\partial t} \quad (1)$$

Where q''' is the heat generation density, k_r is the thermal conductivity in the radial direction, T is temperature, t is time, r is the radius, ρ is the density, and c is the specific heat. Since heat generation only appears in the solid transformer, it can be removed from Eq. (1). q''' will instead be represented as a boundary condition on the inner surface. Since k_r is assumed constant, it can be removed from the brackets and moved to the other side of the equation. Therefore Eq. (1) reduces to:

$$\frac{\partial^2 T}{\partial r^2} + \frac{1}{r} \frac{\partial T}{\partial r} = \frac{1}{\alpha} \frac{\partial T}{\partial t} \quad (2)$$

Notice that α , thermal diffusivity, has been introduced to simplify the equation. Boundary conditions for problem 1 are:

$$-k \frac{\partial T}{\partial r} |_{r_i} = q''' \quad (3)$$

$$-k \frac{\partial T}{\partial r} |_{r_o} = h(T - T_\infty) \quad (4)$$

For simplicity's sake, dimensionless variables are introduced to normalize the equations. They are defined by:

$$\bar{r} = \frac{r}{r_s} \quad (5)$$

$$\bar{T} = \frac{T - T_b}{T_s} \quad (6)$$

$$\bar{t} = \frac{t}{t_s} \quad (7)$$

Where the subscripts s and b represent scales and the base respectively. Applying the normalizing variables to Eq. (1):

$$\frac{T_s}{r_s^2} \frac{\partial^2 \bar{T}}{\partial \bar{r}^2} + \frac{1}{\bar{r} r_s} \frac{T_s}{r_s} \frac{\partial \bar{T}}{\partial \bar{r}} = \frac{1}{\alpha} \frac{T_s}{t_s} \frac{\partial \bar{T}}{\partial \bar{t}}$$

Dividing through by $\frac{T_s}{r_s^2}$ yields:

$$\frac{\partial^2 \bar{T}}{\partial \bar{r}^2} + \frac{1}{\bar{r}} \frac{\partial \bar{T}}{\partial \bar{r}} = \frac{1}{\alpha} \frac{r_s^2}{t_s} \frac{\partial \bar{T}}{\partial \bar{t}}$$

To select the scaling value, r_s , the problem is inspected for important reference geometries. In this case, r_o is of significant importance, so it is chosen to be r_s . Therefore, the equation above becomes:

$$\frac{\partial^2 \bar{T}}{\partial \bar{r}^2} + \frac{1}{\bar{r}} \frac{\partial \bar{T}}{\partial \bar{r}} = \frac{1}{\alpha} \frac{r_o^2}{t_s} \frac{\partial \bar{T}}{\partial \bar{t}}$$

From here, a time scale, t_s is to be selected. Since there is no relevant time scale introduced in the problem statement, t_s is chosen in order to simplify the equation as much as possible. From inspection, choosing t_s to be r_o^2/α simplifies the equation to:

$$\frac{\partial^2 \bar{T}}{\partial \bar{r}^2} + \frac{1}{\bar{r}} \frac{\partial \bar{T}}{\partial \bar{r}} = \frac{\partial \bar{T}}{\partial \bar{t}} \quad (8)$$

Equation (8) represents the normalized 1D heat equation for problem 1. Now the boundary conditions are normalized using the same procedure. Equation (3) becomes:

$$-k \frac{T_s}{r_o} \frac{\partial \bar{T}}{\partial \bar{r}} \Big|_a = q''$$

Where q'' is the heat flux on the inner surface of the sleeve as a result of the heat density, q''' , produced by the transformer. q'' is calculated by:

$$q'' = \frac{q'''V}{A}$$

Since the geometry is assumed 2D, the volume and area of the cylinder are per unit length. Hence, $V = \pi r_i^2$ and $A = 2\pi r_i$. Simplifying:

$$\frac{\partial \bar{T}}{\partial \bar{r}} \Big|_a = -\frac{q'' r_o}{k T_s}$$

Where a is r_i/r_o . T_s is now selected. Since there is no significant temperature scale in the problem, T_s will be chosen to simplify the equation much like the selection of t_s . By choosing T_s to be $q'' r_o/k$ will give:

$$\frac{\partial \bar{T}}{\partial \bar{r}} \Big|_a = -1 \quad (9)$$

Which is the normalized boundary condition on the inner surface of the sleeve. Applying the same procedure to Eq. (4) gives:

$$-k \frac{T_s}{r_o} \frac{\partial \bar{T}}{\partial \bar{r}} \Big|_1 = h(\bar{T} T_s + T_b - T_\infty)$$

The base temperature, T_b is now selected to be T_∞ for simplicity. By plugging in T_s and rearranging, the second normalized boundary condition is:

$$\frac{\partial \bar{T}}{\partial \bar{r}} \Big|_1 = -Bi \bar{T} (\bar{r} = 1) \quad (10)$$

Where Bi , the Biot number has been introduced and is defined by $Bi = h r_o/k$. Redefining the dimensionless variables with the substitutions made above gives:

$$\bar{r} = \frac{r}{r_o} \quad (11)$$

$$\bar{T} = \frac{(T - T_\infty)k}{q'' r_o} \quad (12)$$

$$\bar{t} = \frac{t\alpha}{r_o^2} \quad (13)$$

Therefore, the equations that define a transient solution to problem 1 are represented by Eq. (8) with the boundary conditions Eq. (9-10). Equations (11-13) can be used to reach a solution for $T(r,t)$. In this case,

the problem is analyzed at steady state which removes the time dependence in the equation. Equation (8) is simplified to:

$$\frac{d^2\bar{T}}{d\bar{r}^2} + \frac{1}{\bar{r}} \frac{d\bar{T}}{d\bar{r}} = 0 \quad (14)$$

Rewriting the left hand of Eq. (14):

$$\frac{1}{\bar{r}} \frac{d}{d\bar{r}} \left[\bar{r} \frac{d\bar{T}}{d\bar{r}} \right] = 0$$

Multiplying by r and carrying out the first integration yields:

$$\bar{r} \frac{d\bar{T}}{d\bar{r}} = C1$$

$C1$ represents the constant of integration. Dividing both sides of r and performing the second integration gives the solution for $\bar{T}(\bar{r})$:

$$\bar{T}(\bar{r}) = C1 \ln \bar{r} + C2$$

Applying the boundary conditions as defined by Eq. (9-10) gives the analytical solution to the temperature distribution through the finless sleeve:

$$\bar{T}(\bar{r}) = a \left(\frac{1}{Bi} - \ln \bar{r} \right) \quad (15)$$

To solve for the temperature of the transformer, Eq. (15) is evaluated at r_i :

$$\bar{T} \left(\frac{r_i}{r_o} \right) = \frac{r_i}{r_o} \left(\frac{k}{hr_o} - \ln \frac{r_i}{r_o} \right)$$

Values are then plugged in for the thermal conductivity, convective heat transfer coefficient, and the radii:

$$\bar{T} \left(\frac{r_i}{r_o} \right) = \frac{1.35m}{1.5m} \left(\frac{\frac{170W}{m^2K}}{\frac{30W}{m^2K} * 1.5m} - \ln \frac{1.35m}{1.5m} \right) = 3.49482 \frac{1}{m}$$

T(r) is then found using Eq. (12):

$$3.49482 \frac{1}{m} = \frac{(T - T_{\infty})k}{q''r_o}$$

Again, plugging in for ambient temperature, thermal conductivity, outer radius, and heat flux:

$$3.49482 \frac{1}{m} = \frac{(T - 305K) \frac{170W}{m^2K}}{\frac{1687.5W}{m^2K} * 1.5m}$$

Solving for T gives the analytical solution for the surface temperature of the transformer for problem 1:

$$T(1.35m) = 357.037K$$

2.2 Comparison with Numerical Model

SolidWorks Simulation package is used to numerically calculate the temperature of the sleeve on the inner surface as well as the temperature distribution throughout the sleeve. The geometry used in Fig. 3 is used, Al 6061 is chosen as the material, and boundary conditions are applied. A 2D simplification is used since the temperature is assumed to not vary in the axial direction. Convection is specified on the outside edge of the sleeve as shown in Fig. 6 below.

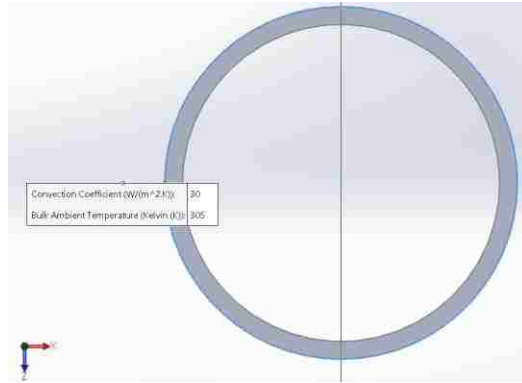


Figure 6: Convection boundary condition on the finless sleeve. Note that $h=30 \text{ W/m}^2\text{-K}$ and the ambient temperature is 305 K.

Similarly, the heat flux boundary condition calculated by $q'' = \frac{q'''V}{A}$ is applied to the sleeve's inner surface which can be seen in Fig. 7.

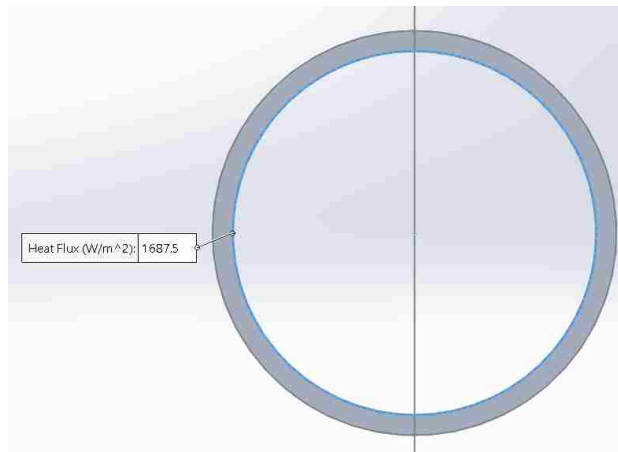


Figure 7: Heat flux boundary condition on the inner sleeve surface. $q''=1687.5 \text{ W/m}^2$.

A mesh for the geometry is now generated in order to solve the numerical calculations. In order to ensure that the results are accurate, the mesh is refined several times until the surface temperature of

the sleeve does not vary with mesh density. Selecting a fine automatic mesh that SolidWorks generates is sufficient for this study. A closeup of the mesh is shown in Fig. 8.

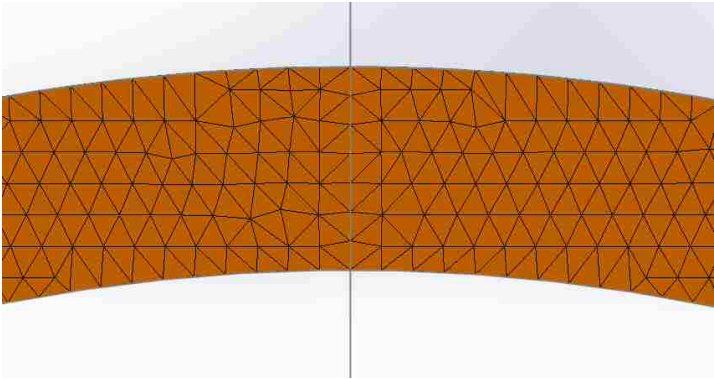


Figure 8: Closeup of the mesh density that is used to calculate the temperature distribution in the finless sleeve. This mesh is dense enough that the temperature no longer changes with a change in mesh size.

The simulation is then run and analyzed for the desired results. Figure 9 shows the temperature distribution throughout the sleeve on the geometry.

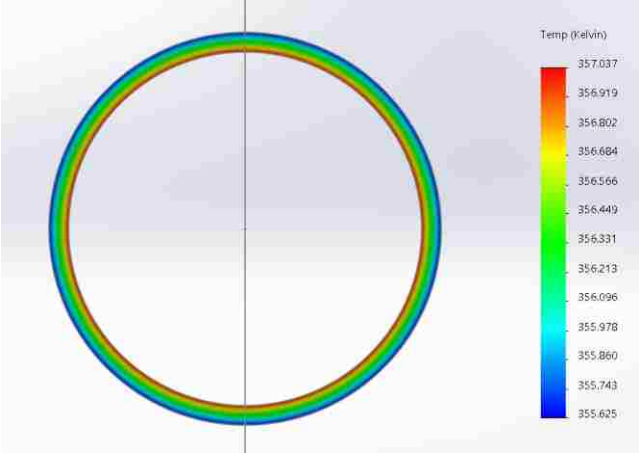


Figure 9: Finless sleeve temperature distribution shown on the model geometry.

Inspection of Fig. 9 shows that the maximum temperature occurs on the inner surface of the sleeve. This value of 357.037 K is identical to the analytical solution obtained in the previous section. In order to confirm that the numerical simulations and analytical solution are the same, the temperature from the simulations are plotted against the analytical solution at the same radius. The values of the temperature in the sleeve are obtained in SolidWorks by “probing” along the radius. Table 1 lists the result of this probe.

Table 1: Temperature as a function of z (radius) for the finless sleeve from SolidWorks Simulation.

Node	Value (Kelvin)	X (m)	Y (m)	Z (m)
395	357.037	0	0	-1.35
4250	356.931	0	0	-1.36071
396	356.826	0	0	-1.37143
4248	356.722	0	0	-1.38214
397	356.618	0	0	-1.39286
4245	356.516	0	0	-1.40357
398	356.413	0	0	-1.41429
4242	356.313	0	0	-1.425
399	356.212	0	0	-1.43571
4240	356.113	0	0	-1.44643
400	356.013	0	0	-1.45714
4237	355.916	0	0	-1.46786
401	355.818	0	0	-1.47857
5427	355.721	0	0	-1.48929
1	355.625	0	0	-1.5

Figure 10, a snip of an excel worksheet, shows how the values of T_{bar} and subsequently $T(r)$ are obtained analytically using (15).

	A	B	C	D	E	F	G	H	I
1									
2	tamb	r0	h	k	a	q''	r	tbar	t
3	305	1.5	30	170	0.9	1687.5	1.35	/\$B\$3)	357.0369
4							1.360714	3.48771	356.931
5							1.371429	3.480651	356.8259
6							1.382143	3.473647	356.7216
7							1.392857	3.466697	356.6181
8							1.403571	3.459801	356.5154
9							1.414286	3.452956	356.4135
10							1.425	3.446164	356.3124
11							1.435714	3.439422	356.212
12							1.446429	3.432731	356.1124
13							1.457143	3.426089	356.0135
14							1.467857	3.419495	355.9153
15							1.478571	3.41295	355.8178
16							1.489286	3.406452	355.7211
17							1.5	3.4	355.625

Figure 10: Analytical calculation of T for the values of r that correspond to the locations of the probe in table 1.

When the numerical and analytical results are plotted together, it is clear that the simulation has been validated. Figure 11 below shows the graph of the comparison.

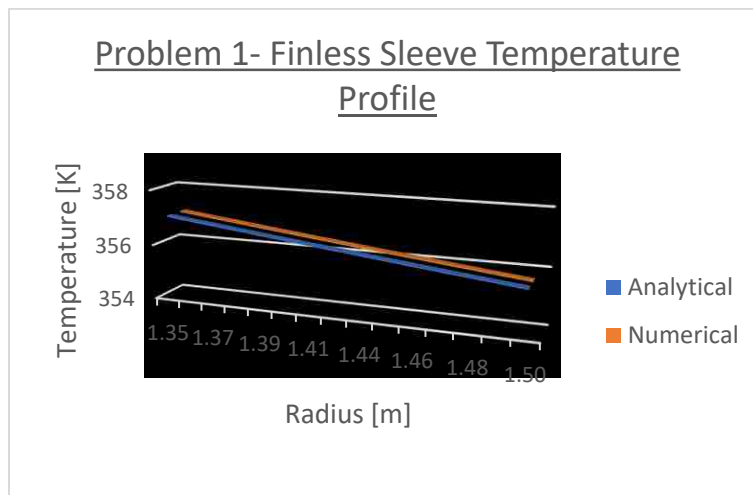


Figure 11: Graph of analytical vs numerical data for the finless sleeve shows that the simulation is indeed validated.

3. 3D Numerical Simulation Setup

Since the 2D simulation has been validated analytically using the heat equation, work can begin on the 3D simulations. In SolidWorks Flow Simulation 2016, the Project Wizard is used to aide in the setup of the problems. The first step in the Wizard is to select the unit system in which the problem will be solved. The default unit system of SI (m-kg-s) is chosen for simplicity. Next, several options are presented to most accurately represent the problem. In this case, external flow is chosen since air will be flowing over the outside of the transformer. Heat conduction in solids is selected since the transformer is generating heat. Most importantly, gravity is turned on in the y-direction to introduce the buoyancy effects of the fluid as it is heated by the transformer, thus driving the natural convection. Figure 12 below shows this step in the Wizard.

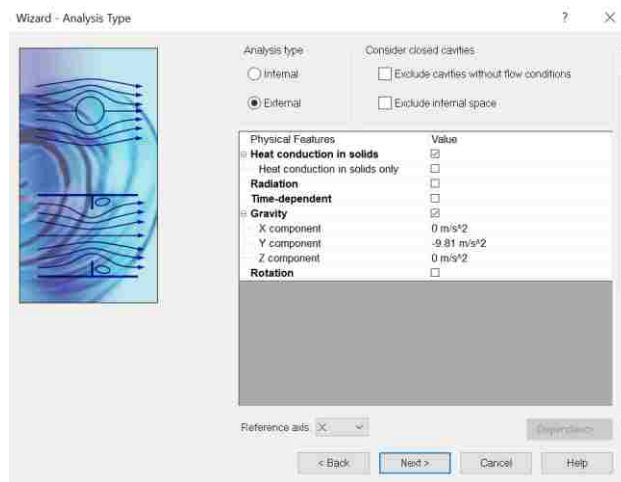


Figure 12: Simulation Wizard selections for analysis type. Gravity is in the y-direction.

Next, the default fluid of the simulation is chosen, which in this case is air. The flow characteristics are also chosen to be laminar and turbulent, meaning that SolidWorks will define turbulence parameters

which will be introduced if the flow enters the turbulent regime. This strategy will be discussed more in later sections. Once the fluid has been selected, the default solid is selected. Aluminum 6061 alloy is chosen as the material for the transformer; material properties as defined by SolidWorks were introduced in Fig. 5. These selections are important since the program will be using the built-in material properties to properly model the heat conduction through the solid as well as the flow around the transformer. Wall roughness can now be added to the simulation, but in this case the value is kept at zero. Future work could investigate the effects of wall roughness on the flow between the fins. Finally, initial and ambient conditions are selected. Figure 13 shows the selections for these simulations.

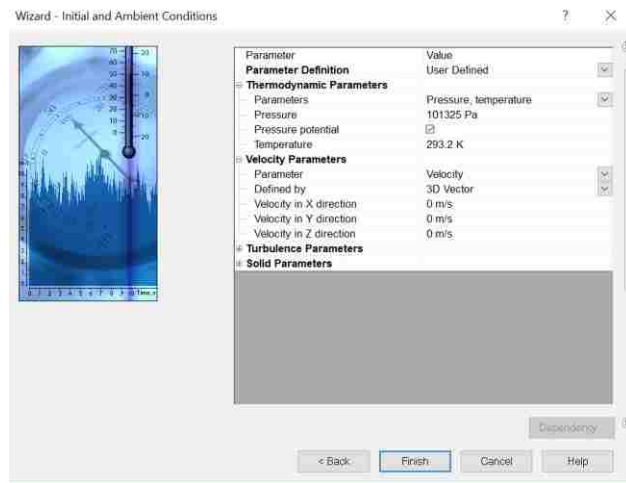


Figure 13: Initial conditions for the transformer in natural convection. Ambient temperature and pressure are chosen as 293.2 K and 101325 Pa- atmospheric conditions. Zero velocity parameters are defined to model still air that is only affected by the transformer heat.

Now that all the steps have been completed in the Simulation Wizard, the project has been generated. The default computational domain for the simulation can be seen in Fig. 14 below. This default scenario of 22x22m is unnecessarily large for this simulation, so the computational domain is reduced manually. Symmetry boundary conditions are imposed in the x and z-directions in order to greatly reduce

the computational space, while the domain in the y-direction is kept sufficiently large enough to properly model the flow that will be induced from natural convection. Figure 15 shows the domain once these simplifications have been applied.

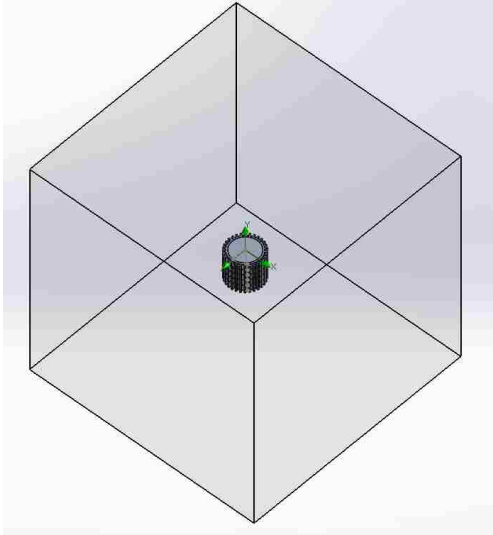


Figure 14: Default computational domain generated by the Flow Simulation package is far too large for a calculation with a dense mesh.

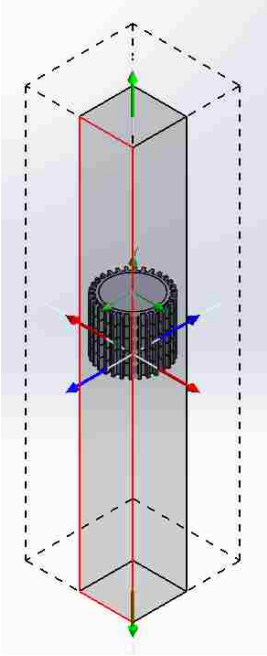


Figure 15: Computational domain with simplifications. The shaded grey region is the actual volume that is used in calculations, and the dashed region represents the total volume that is reduced by the use of symmetry in the x and z-directions.

With the computational domain properly defined, the next option in the Flow Simulation Analysis tree, shown in Fig. 16, is completed.

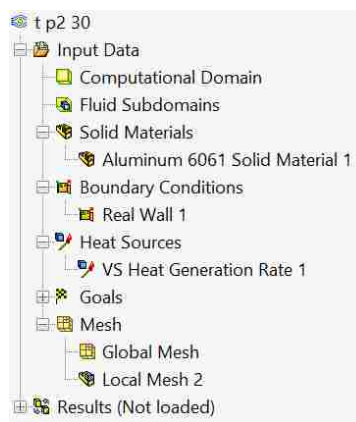


Figure 16: Flow Simulation Analysis tree used to generate the appropriate conditions for the simulation. No fluid subdomains are defined since the entire fluid domain is assumed to be air.

Boundary condition options in the Simulation package include flow openings, where inlet velocities or mass flow rates can be defined, pressure openings of environmental or static pressure, and wall conditions. Since the transformer is in open space without any implied flow conditions, the only boundary condition applied is the real wall condition to the entire surface of the solid. Wall parameters are defined as the default value of 293.2 K, the ambient temperature, a roughness value of zero micrometers, and a heat transfer coefficient that is also kept at zero. If there was a constant heat flux over the entire outside boundary of the solid, the heat transfer coefficient parameter could be defined, but since it is assumed that the value will vary in the y-direction, it is kept at the default value.

Heat sources are now added to the problem. Since only the transformer is generating heat, a volumetric heat generation source of 2500 W is applied to the cylindrical volume only, not the sleeve with fins. This source is highlighted below in Fig. 17. As discussed earlier in the analytical solution, this volumetric source could be simplified into a heat flux boundary condition on the inner surface of the sleeve if the problem is to be evaluated at steady-state only. For these 3D simulations, the volumetric heat density is kept as the heat source in order to maintain the geometric volume of the transformer.

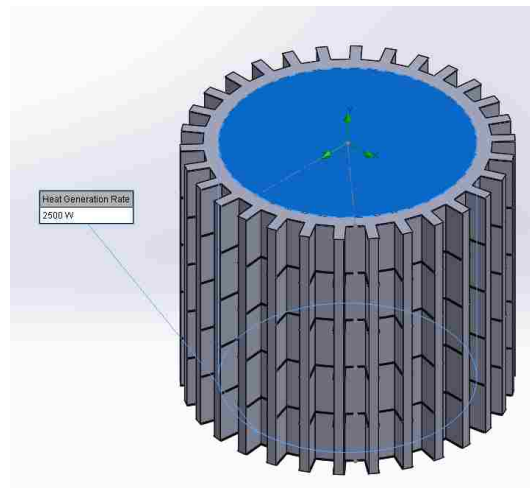


Figure 17: Heat Generation Rate of 2500 W applied to the transformer volume.

The next section of the simulation tree, goals, are now to be chosen. These goals will be output in the calculations and can be chosen as convergence criteria to ensure that the values generated are of sufficient accuracy. There are hundreds of potential goals that can be selected in the global domain, on surfaces, at points in the model, or over volumes in the model. Some goals that can be selected are temperatures, velocities, Mach numbers, pressures, densities, turbulence parameters, normal forces, shear forces, torques, etc. The list of goals chosen for these simulations is shown below in Fig. 18.

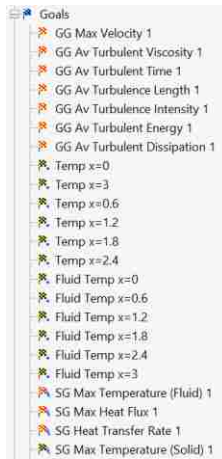


Figure 18: Goals selected for each of the simulation studies.

The first group of goals, beginning with GG represent global goals that will be tracked over the entire computational domain. Max velocity is chosen to examine the change in flow velocities over the three different pin configurations. Global turbulent parameters are chosen for some insight into how the application deals with turbulent regimes. Next, the temperature of the solid and the surrounding fluid temperature is chosen at the surface of each of the small pins. These values will be used to calculate the Rayleigh number for the natural convection to determine where the transition to the turbulent regime takes place. Then, surface goals of maximum solid and fluid temperature, max heat flux, and max heat transfer rate are chosen on the surfaces between the fins. These values are chosen to observe the change in temperatures with the number of fins. Finally, the last goal that doesn't appear in the list shown in Fig. 18 is the maximum temperature of the transformer volume. This is the main goal of the simulations and will be used as the main criteria for evaluating the different configurations.

The last, and arguably most important step in the simulation setup is to define the mesh used for calculations. Selections for the mesh will be given in this section, but a more in-depth review of the meshing process and optimization will be given in the next section. As seen in Fig. 16, 2 different meshes

are generated. The first, a global mesh, defines the level of initial mesh for the entire computational domain. For these studies, a level of 3 out of a possible 7 is selected, and the option of uniform mesh is chosen. This very basic mesh will comprise the whole domain of the problem for both fluidic and solid cells. Next, a local mesh is generated around the transformer solid. The program gives several options on how to define the location of the local mesh- a cuboid region is chosen for these simulations. Figure 19 below shows the local mesh highlighted in green around the transformer solid.

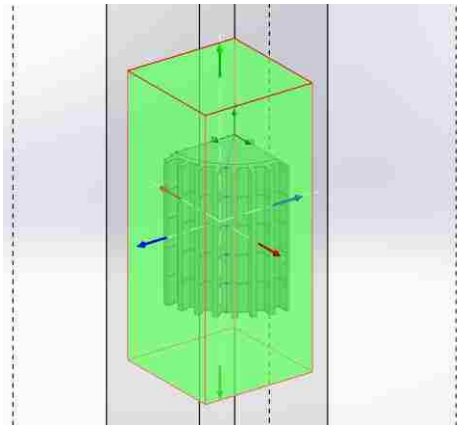


Figure 19: Local mesh defined by a rectangular prism that encompasses the entire transformer solid with adequate surrounding fluid volume. This region will be more greatly refined to improve calculation results.

There are several options for refining the mesh in the local region including refining solid cells, fluidic cells, and cells on the fluid/solid boundary. Advanced refinements are used in order to generate more cells around the small solid features of the horizontal pins. A manual parametric study was conducted in order to determine the minimum mesh size necessary to reach convergence in the simulation goals. This parametric study and other mesh topics will be discussed in greater detail in later chapters. Once the mesh has been generated that will produce accurate results, the simulation setup is complete and calculations can now begin.

3.1 Mesh Independence Parametric Studies

In order to prove that the results generated by the simulations are accurate, a mesh independence study has to be performed. This involves running the calculations with meshes of increasing density until the values of the goals no longer change with the number of cells. At first, this was done manually by creating meshes of varying density while keeping all other inputs constant. It was found that the fluid temperature and velocity at points between the fins tended to vary more drastically than the temperature of the solid, so these goals were chosen as the criteria for convergence in the parametric studies. While the temperature of the solid stopped varying with cell count at around 2.5 million cells, the fluid velocity and temperature took longer to converge as shown in Fig. 20-21 below.

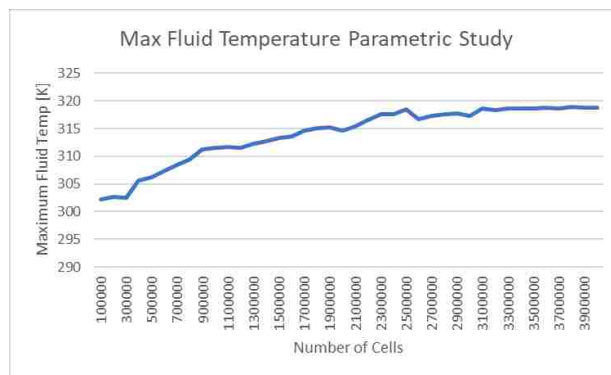


Figure 20: Parametric study of the maximum fluid temperature as a function of number of cells.

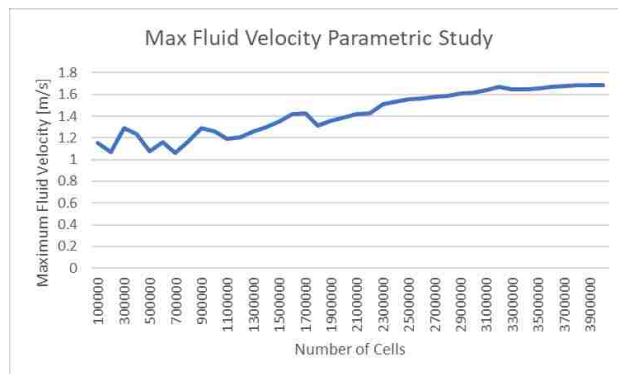


Figure 21: Parametric study of the maximum fluid velocity as a function of number of cells.

From the graphs, there is significant change in both the fluid temperature and velocity before the number of cells approaches 4,000,000. This number will now be the base value used for each mesh to ensure that the solution is independent of the grid density.

4. SolidWorks Flow Simulation

4.1 Mesh Generation

This chapter will discuss mesh generation, calculation format, and boundary layer treatment as defined in the White Paper which was presented at the NAFEMS World Congress 2013 [17]. SolidWorks Flow Simulation is a finite-volume based CFD program that models fluid flow using the Navier-Stokes equations. This program is an add-on to the regular SolidWorks package, that is used to generate the CAD model of the geometry.

Mesh generation is accomplished by using Cartesian-based meshes that are independent of the model geometry. This technique generates cubic cells that are adjacent to each other as well as the boundary of the computational domain. The cells are also oriented along the Cartesian coordinates of the CAD geometry. Since Cartesian-based meshes cannot generally form fit to the surfaces of the geometry, partial cells consisting of fluid and solid volume will be generated at the fluid/solid boundary. The mesh can then be refined by splitting the cubic cells into a maximum of 8 similarly shaped cuboids to properly represent surface boundaries of the geometry. Since the CAD model is native to the program, it can easily identify solid edges or boundaries of the solid model and can then refine the mesh more accurately. These refinements can be done manually as was illustrated in the previous section with the mesh independence parametric studies, or this process can be automated by built in SolidWorks functions that will be discussed in detail later in the chapter.

4.2 Flow Simulation Equations

Once a suitably dense mesh has been generated, each individual cell, or control volume, is ready for calculation. First, the area and normal vector direction for each face of each cell are calculated using

the CAD geometry. Then the appropriate equations can be applied to the cells depending on their type- fluid flow equations for fluidic cells, and heat conduction and direct electrical current for solid cells.

Navier-Stokes equations are used to formulate the fundamental conservation laws of mass, momentum, and energy as seen below in Eq. (16-19):

$$\frac{\partial \rho}{\partial t} + \frac{\partial(\rho u_i)}{\partial x_i} = 0 \quad (16)$$

$$\begin{aligned} \frac{\partial(\rho u_i)}{\partial t} + \frac{\partial}{\partial x_j}(\rho u_i u_j) + \frac{\partial P}{\partial x_i} = \\ \frac{\partial}{\partial x_j}(\tau_{ij} + \tau_{ij}^R) + S_i \end{aligned} \quad (17)$$

$$\begin{aligned} \frac{\partial \rho H}{\partial t} + \frac{\partial \rho u_i H}{\partial x_i} = \frac{\partial}{\partial x_i}(u_j(\tau_{ij} + \tau_{ij}^R) + q_i) + \frac{\partial p}{\partial t} \\ - \tau_{ij}^R \frac{\partial u_i}{\partial x_j} + \rho \epsilon + S_i u_i + Q_H \end{aligned} \quad (18)$$

Where H is defined by:

$$H = h + \frac{u^2}{2} \quad (19)$$

These equations are then supplemental equations of state, and by empirical relationships for density, viscosity, and thermal conductivity as a function of temperature in order to describe the flow. Since the program deals with laminar and turbulent regimes, a turbulence closure model must be used. Local Reynolds numbers, defined in Eq. (20), are used to determine whether the flow is laminar or turbulent.

$$Re = \frac{uL}{\nu} \quad (20)$$

Where uL is the product of scaled velocity and length, and ν is the kinematic viscosity of the fluid. Favre-averaged Navier-Stokes equations are used to predict the effects of turbulent flows; time-averaged effects of turbulence on the flow are measured, while large-scale, time-dependent phenomena are taken into account directly. Using this procedure generates a 9x9 matrix comprised of criteria known as Reynolds Stresses. In order to solve this large system of equations, a turbulence closure scheme must be used. SolidWorks Flow Simulation calculates the turbulent kinetic energy and dissipation rate using the k- ϵ model to solve the system of Reynolds Stresses.

A more accurate model to predict wall turbulence using the k- ϵ model was developed by Lam and Bremhorst [18] incorporates damping functions into the following turbulence conservation laws:

$$\frac{\partial \rho k}{\partial t} + \frac{\partial \rho k u_i}{\partial x_i} = \frac{\partial}{\partial x_i} \left(\left(\mu + \frac{\mu_t}{\sigma_k} \right) \frac{\partial k}{\partial x_i} \right) + \tau_{ij}^R \frac{\partial u_i}{\partial x_j} - \rho \epsilon + \mu_t P_B \quad (21)$$

$$\frac{\partial \rho \epsilon}{\partial t} + \frac{\partial \rho \epsilon u_i}{\partial x_i} = \frac{\partial}{\partial x_i} \left(\left(\mu + \frac{\mu_t}{\sigma_\epsilon} \right) \frac{\partial \epsilon}{\partial x_i} \right) + C_{\epsilon 1} \frac{\epsilon}{k} \left(f_1 \tau_{ij}^R \frac{\partial u_i}{\partial x_j} + C_B \mu_t P_B \right) - f_2 C_{\epsilon 2} \frac{\rho \epsilon^2}{k} \quad (22)$$

$$\tau_{ij} = \mu s_{ij} \quad (23)$$

$$\tau_{ij}^R = \mu_t s_{ij} - \frac{2}{3} \rho k \delta_{ij} \quad (24)$$

$$s_{ij} = \frac{\partial u_i}{\partial x_j} + \frac{\partial u_j}{\partial x_i} - \frac{2}{3} \delta_{ij} \frac{\partial u_k}{\partial x_k} \quad (25)$$

$$P_B = - \frac{g_i}{\sigma_B} \frac{1}{\rho} \frac{\partial \rho}{\partial x_i} \quad (26)$$

Where the following coefficients are defined as:

$$C_\mu = 0.09$$

$$C_{\epsilon 1} = 1.44$$

$$C_{\epsilon 2} = 1.92$$

$$\sigma_k = 1$$

$$\sigma_\epsilon = 1.3$$

$$\sigma_B = 0.9$$

$$C_B = 1 \text{ if } P_B > 0, C_B = 0 \text{ if } P_B < 0$$

The turbulent viscosity is found by using Eq. (27):

$$\mu_t = f_\mu \cdot \frac{C_\mu \rho k^2}{\epsilon} \quad (27)$$

The damping function proposed by Lam and Bremhorst is found with:

$$f_\mu = (1 - e^{-0.025R_y})^2 \cdot \left(1 + \frac{20.5}{R_t}\right) \quad (28)$$

Where:

$$R_y = \frac{\rho \sqrt{k} y}{\mu} \quad (29)$$

$$R_t = \frac{\rho k^2}{\mu \epsilon} \quad (30)$$

Here y is the distance from a point to the wall. Finally, the damping functions f_1 and f_2 are determined by:

$$f_1 = 1 + \left(\frac{0.05}{f_\mu}\right)^3 \quad (31)$$

$$f_2 = 1 - e^{-R_t^2} \quad (32)$$

These damping functions, f_1 , f_2 , and f_μ decrease the turbulent viscosity and turbulence energy and increase turbulence dissipation rate when the Reynolds number defined in Eq. (29) becomes too small. When the damping functions equal 1, the calculations revert back to the original k- ϵ model. Lastly, the heat flux is defined by:

$$q_i = \left(\frac{\mu}{Pr} + \frac{\mu_t}{\sigma_c} \right) \frac{\partial h}{\partial x_i}, i = 1,2,3 \quad (33)$$

Where the constant $\sigma_c=0.9$, Pr is the Prandtl number, and h is enthalpy. In combination, Eq. (16-33) accurately model the flow characteristics in either the laminar or turbulent regime without the need to specify initial conditions.

Solid regions in SolidWorks Flow Simulation are subjected to both heat conduction and direct electrical current, producing Joule heating that will be used as a source of heat in the energy equation described in Eq. (18,19). Since there is no electrical heating modeled in these simulations, only conduction will be considered. Heat conduction through the solid material is described by Eq. (34):

$$\frac{\partial \rho e}{\partial t} = \frac{\partial}{\partial x_i} \left(\lambda_i \frac{\partial T}{\partial x_i} \right) + Q_H \quad (34)$$

Where e represents the internal energy, defined by the specific heat of the material multiplied by the absolute temperature. Q_H is defined by the specific heat release or absorption rate per unit volume. λ_i are the eigenvalues of the thermal conductivity tensor which is considered diagonal for an isotropic material. Therefore $\lambda_1 = \lambda_2 = \lambda_3 = \lambda$.

4.3 Boundary Layer Treatment

Cartesian based meshes have proven effective at managing CAD data in an efficient and robust manner, but struggle to resolve boundary layers on coarse meshes. The following approaches seek to minimize this shortfall and accurately describe the flow close to walls. Since the mesh at the solid/fluid boundary may be too coarse for the application of the complete Navier-Stokes equation, the Prandtl approach for boundary layers is used to ensure that the boundary layer region is properly defined.

SolidWorks incorporates an original approach called the Two-Scale Wall Function (2SWF) to couple the boundary layer calculations with the flow solution outside of the boundary layer. In the regions where the number of cells across the boundary layer is inadequate for direct calculations, a “thin” boundary layer treatment is used. Alternatively, when the boundary layer thickness can be properly described by the number of cells, a “thick” boundary layer treatment can be used. These 2 approaches have been thoroughly vetted and were validated by Balakine et al. [19].

For “thin” boundary layers, the Prandtl equations are solved along fluid streamlines spanning from the wall to the boundary layer thickness, δ . In the case of laminar flow conditions, these equations are solved along with Shvets trial functions technology which was introduced in by Ginzburg [20]. Turbulent or transitional boundary layers are more complex and require more approximations to reach a solution. In this case, the Van Driest hypothesis of mixing length is used [21]. Roughness, which isn’t considered for these simulations, and turbulence from outside flow rely on semi-empirical relations to define their effect on the boundary layer and correct the wall shear stress and heat flux from the fluid to the wall. Compressibility, turbulent kinetic energy dissipation, and body forces are treated in a similar fashion. Using these calculations, the boundary layer thickness, wall shear stress, and heat flux from the fluid to the wall are obtained for use as boundary conditions for the Navier-Stokes equations. Conditions for the k- ϵ model near the wall are defined by:

$$\frac{\partial k}{\partial y} = 0 \quad (35)$$

$$\epsilon = \frac{C_{\mu}^{0.75} k^{1.5}}{ky} \quad (36)$$

In the other case, when there are enough cells to correctly calculate the boundary layer, Navier-Stokes equations can be used directly in the laminar flow regime. When turbulence is present, a modified version of the wall function that uses the profile defined by Van Driest rather than a simple logarithmic velocity profile. Eq. (37) describes this profile:

$$u^+ = \int_0^{y^+} \frac{2 \cdot d\eta}{1 + \sqrt{1 + 4 \cdot K^2 \cdot \eta^2 \cdot \left[1 - \exp\left(-\frac{\eta}{A_v}\right)\right]^2}} \quad (37)$$

Where $K=0.4054$ is the Karman constant, and $A_v=26$ is the Van Driest coefficient. Equations (35-37), when coupled with the general Navier-Stokes equations, sufficiently model boundary layer conditions for cells that are near to walls.

4.4 Flow Simulation Adaptive Mesh

SolidWorks Flow Simulation has a built in adaptive mesh technique that greatly cuts down the amount of time that is required to ensure an accurate solution that is grid independent. Rather than performing numerous parametric studies that relate the number of cells in the study to a particular goal, the program splits the cells in high-gradient flow regions and merges the cells in low-gradient regions based on the results of the calculations described in the previous section. In order for the program to track the regions where mesh refinement is required, indicator functions for the mass, energy, and species conservation laws (C_m, C_p, C_e, C_y) are required. These indicators are used to determine where the location

truncation error (LTE) is large enough to justify a mesh refinement or small enough to coarsen the mesh.

The indicator function for the momentum conservation is expressed as:

$$C_m = \Gamma \left(\frac{\eta}{\eta_{min}}, foam \right) \cdot h \cdot S \quad (38)$$

$$\Gamma = 1 + \left(\frac{\eta}{\eta_{min}} - 1 \right) \cdot foam \quad (39)$$

Where $S = \sqrt{0.5 \cdot S_{ij} \cdot S_{ij}}$ is a convolution of the strain rate tensor, η is the total number of adjacent cells, η_{min} is the number of the coordinate directions in which at least one cell is an adjacent cell, $foam$ is the cell level gap displacement factor, which shifts the region where the mesh cells must be split to the area where the LTE is definitely small, and h is the characteristic cell size defined by:

$$h = \frac{\sum_{i \neq j} \sum_j \left| \frac{\partial u_i}{\partial x_j} \right| h_j}{\sum_{i \neq j} \sum_j \left| \frac{\partial u_i}{\partial x_j} \right|} \quad (40)$$

Where u represents the fluid velocity. The indicator functions for the mass, energy, and species conservation laws are shown in Eq. (41-43):

$$C_\rho = \Gamma \cdot \left[\sum_i \left(\frac{1}{\rho} \frac{\partial \rho}{\partial x_i} h_i \right)^2 \right]^{\frac{1}{2}} \quad (41)$$

$$C_e = \Gamma \cdot \left[\sum_i \left(\frac{1}{T} \frac{\partial T}{\partial x_i} h_i \right)^2 \right]^{\frac{1}{2}} \quad (42)$$

$$C_y = \Gamma \cdot \left[\sum_i \left(\frac{\partial y}{\partial x_i} h_i \right)^2 \right]^{\frac{1}{2}} \quad (43)$$

Once the indicator functions have been calculated, they are then compared to limiting values which are determined automatically for each refinement cycle. Mesh splitting or merging will then take

place depending on how the calculated indicator functions compare with the automatically generated limiting values.

The adaptive mesh procedure as defined in Eq. (38-43) takes place in the background of the flow simulation program with minimal input from the user. Certain variables are available to control the refinement process which are presented by SolidWorks in the flow simulation calculation control options, shown below in Fig. 22.

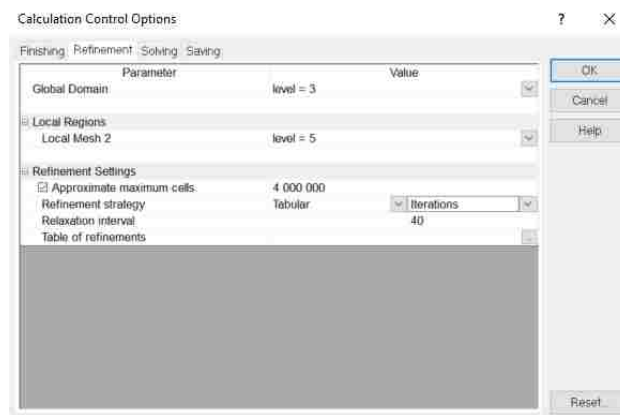


Figure 22: Calculation Control Options dialogue box used to specify criteria for the adaptive mesh refinements.

The first settings to be adjusted are the maximum refinement level for each mesh. Values of 3 and 5 are chosen for the global and local meshes respectively. Recalling the information on mesh refinement presented in the beginning of the chapter, this means that the Cartesian-based cuboid geometry of the mesh cells can be split 3 times in the global domain and 5 times in the local region surrounding the transformer volume. Next, the approximate maximum cells is set to a value of 4,000,000 which was determined to be required mesh density to reach convergence in the fluid temperature and velocity as graphed in Fig. 18. Therefore, the mesh refinement process will not produce meshes that have greater than 4,000,000 cells. Several options are available for the refinement strategy- tabular, periodic, or manual only refinement. Periodic refinement allows the user to specify the moment of first refinement

in the calculation process as a value of travels through the whole model or as iterations. A period is then chosen over which the subsequent refinements will take place. Manual only refinements removes scheduled refinements and relies on user input to start the refinement process. Tabular refinement, which is used in these simulations, uses a table of refinements specified by the user. Like the periodic refinements, either travels or number of iterations are chosen as variables to begin the mesh refinement. The relaxation interval is the amount of travels or iterations that must take place after the last refinement has taken place, ensuring that the calculation has enough time to reach convergence with the newly adapted mesh. Using the calculation control options and adaptive mesh refinement significantly reduced the amount of time spent on generating and running each simulation.

5. Results

5.1 Adaptive Mesh

Figures 23-25 show the resulting mesh that SolidWorks generated using the adaptive mesh technique. The mesh generated is dense enough to capture the flow velocities and temperatures through the transformer fins with great accuracy. Notice the area of increased refinement above the transformer where the fluid velocities are maximized, generating the largest divergences. The curved profile of the yellow region, denoting a refinement of 4 from the original global mesh, is generated to better compute the flow at the top of the transformer. At this location, the flow begins to recirculate before continuing in the vertical direction. This phenomenon will be examined more carefully in the subsequent section.

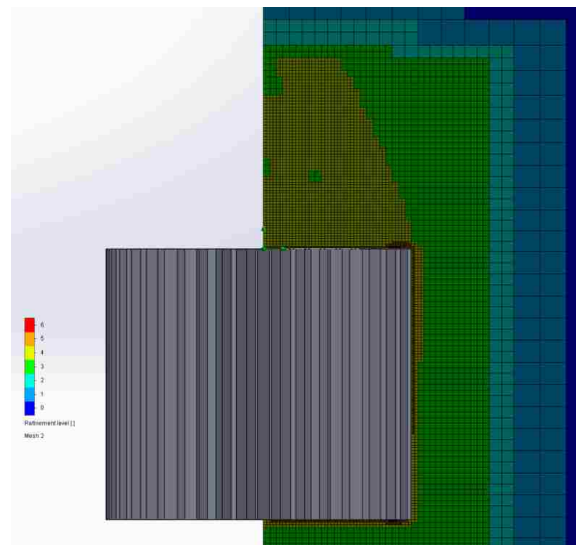


Figure 23: Adaptive mesh generated for the fluid region for the simple transformer with 40 fins and no pins.

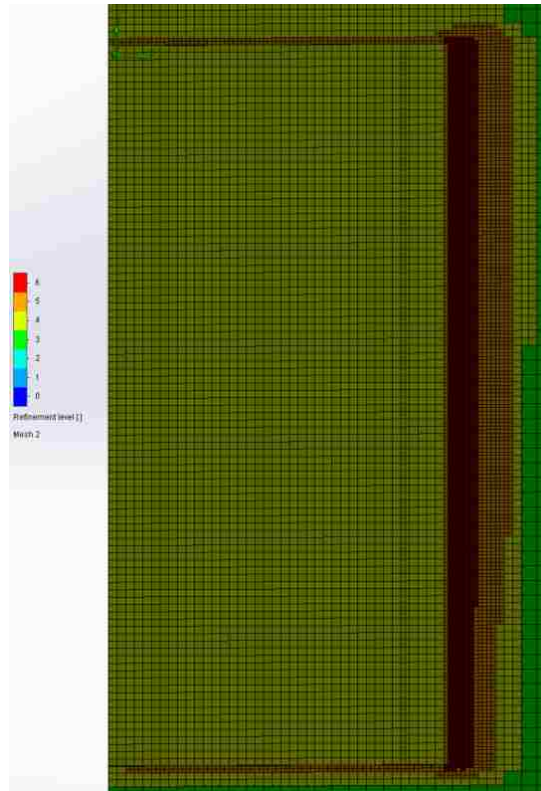


Figure 24: Close up of the mesh with the model geometry hidden. The orange and red sections show the increased mesh density at the fluid/solid boundary in the fin channels.

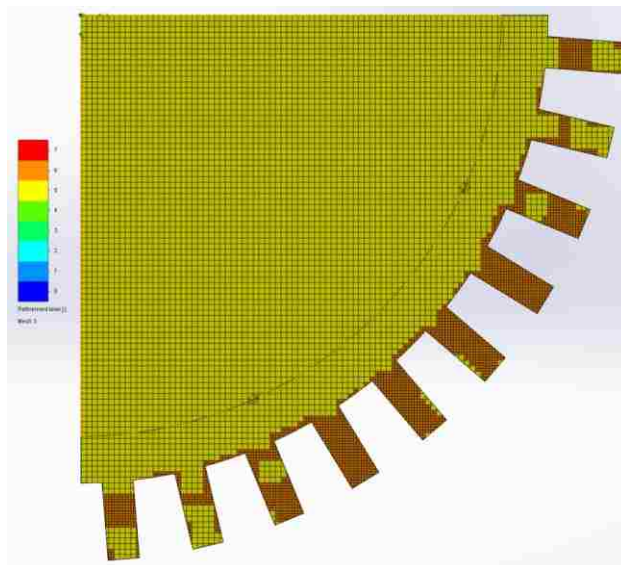


Figure 25: Mesh generated on the solid transformer fins.

5.2 Fluid Velocity

As expected, the fluid surrounding the transformer will be heated by the surface and begin to rise, driven only by natural convection. Each simulation saw similar flow fields; air velocity increases along the fin channels from the bottom of the transformer until it reaches the top edge. At this point the air begins to recirculate and form an eddy at the top surface of the transformer. Figures 26-27 show the flow trajectories for the default transformer, with every face acting as a starting point for the fluid particles. Figures 28-29 show the same for configuration 1, but in this case only the surfaces on and between 3 fins are chosen as fluid starting points to contrast with the other images. Finally, Fig. 30-31 show the trajectories for configuration 2. In each figure, the color of the arrows represents the temperature of the fluid. The images clearly show surrounding air at the initial temperature of 293 K being drawn toward the base of the transformer. Once the air contacts the sleeve surface, the temperature immediately begins to rise. The temperature and velocity of the air increases as it travels up the fin channels until it reaches the top edge. This sudden change of geometry causes the flow field to break down and causes recirculation on the top section of the transformer. The majority of the fluid then travels straight up due to natural convection from the top of the transformer since it is less dense than the surrounding air.

Cut plots showing the fluid velocity through the fin channels are shown next in Fig. 32-33. The plots are both for sleeves with 40 fins- Fig. 32 is of configuration 2 which is compared to the default sleeve in Fig. 33. There is a clear difference in how the how velocity develops around the transformers when examined side by side. The velocity profile for the default configuration is steady and consistent, increasing to the maximum velocity shown in Fig. 33 at the top edge of the transformer. Alternatively, the velocity profile for configuration 2 is much less uniform. Disturbances in the flow from the horizontal pins are evident and cause an increase in velocity that radiates outwards from the sleeve surface. Figure 34, a close up of the flow velocity around the pins, shows detail of these disturbances. There are also small

regions just beyond the pins where the velocity approaches zero. Despite these regions of low velocity along the sleeve surface, the velocity at the top edge of the transformer reaches a higher value than that of the default configuration. This increased velocity at the top edge and from the disturbances caused by the pins are factors that prove to amplify heat transfer.

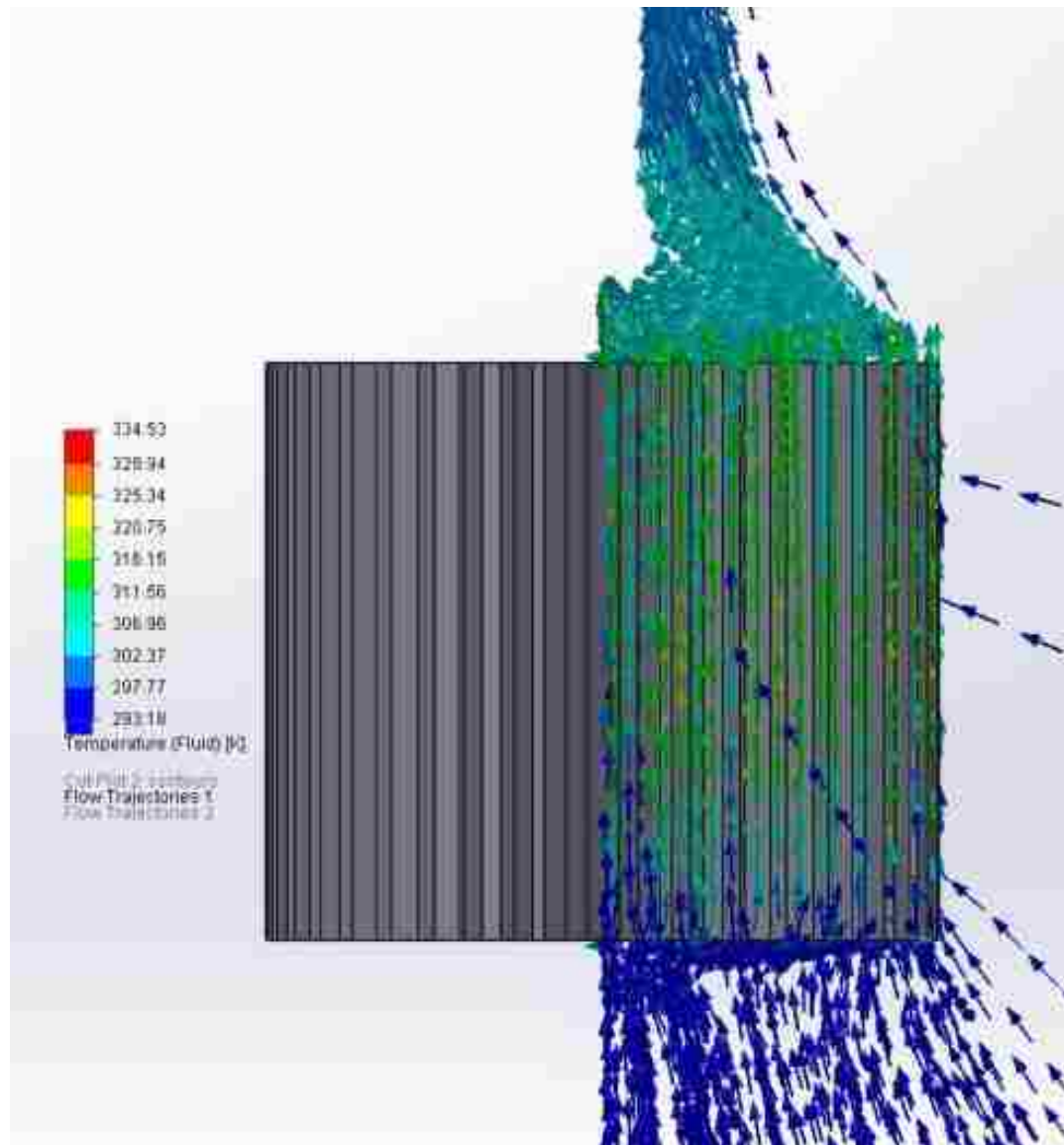


Figure 26: Flow trajectory for the default transformer with 40 fins.

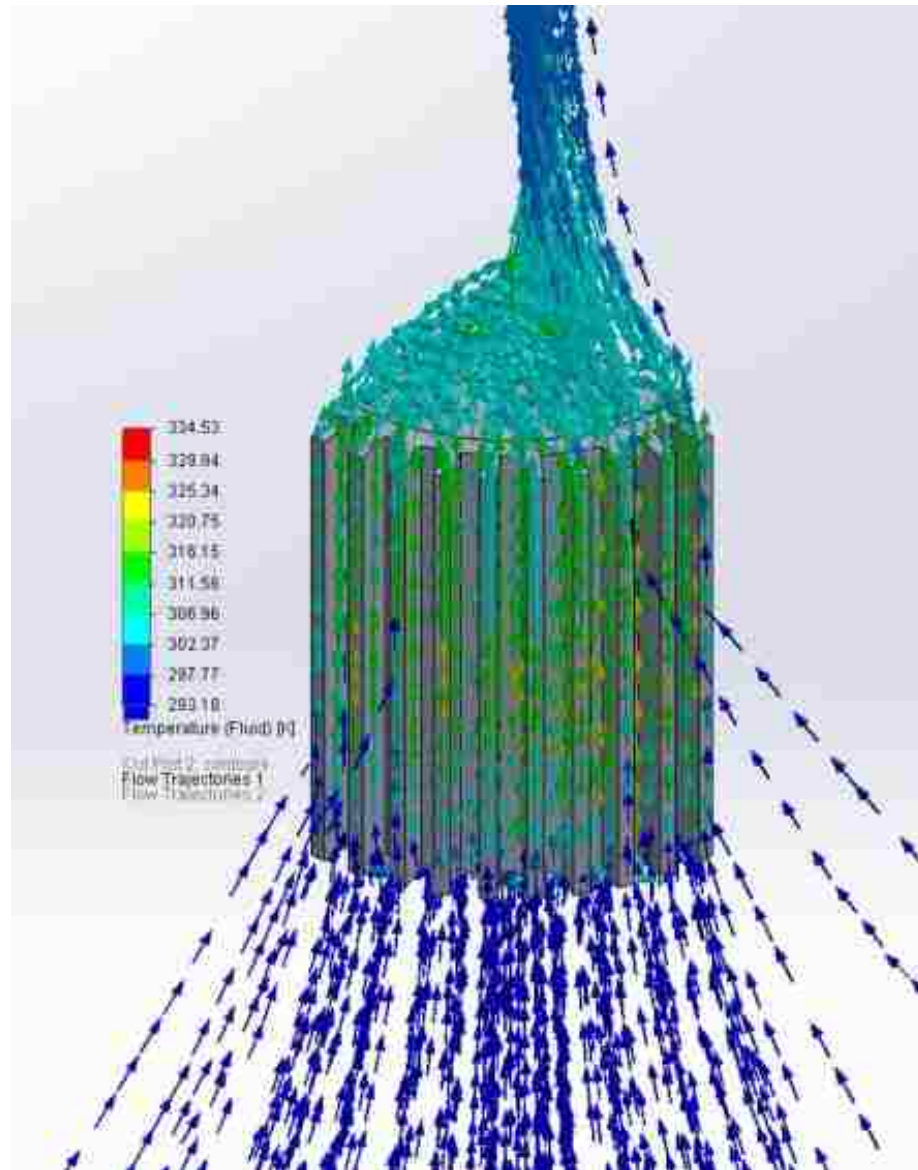


Figure 27: Isometric view of Fig. 28.

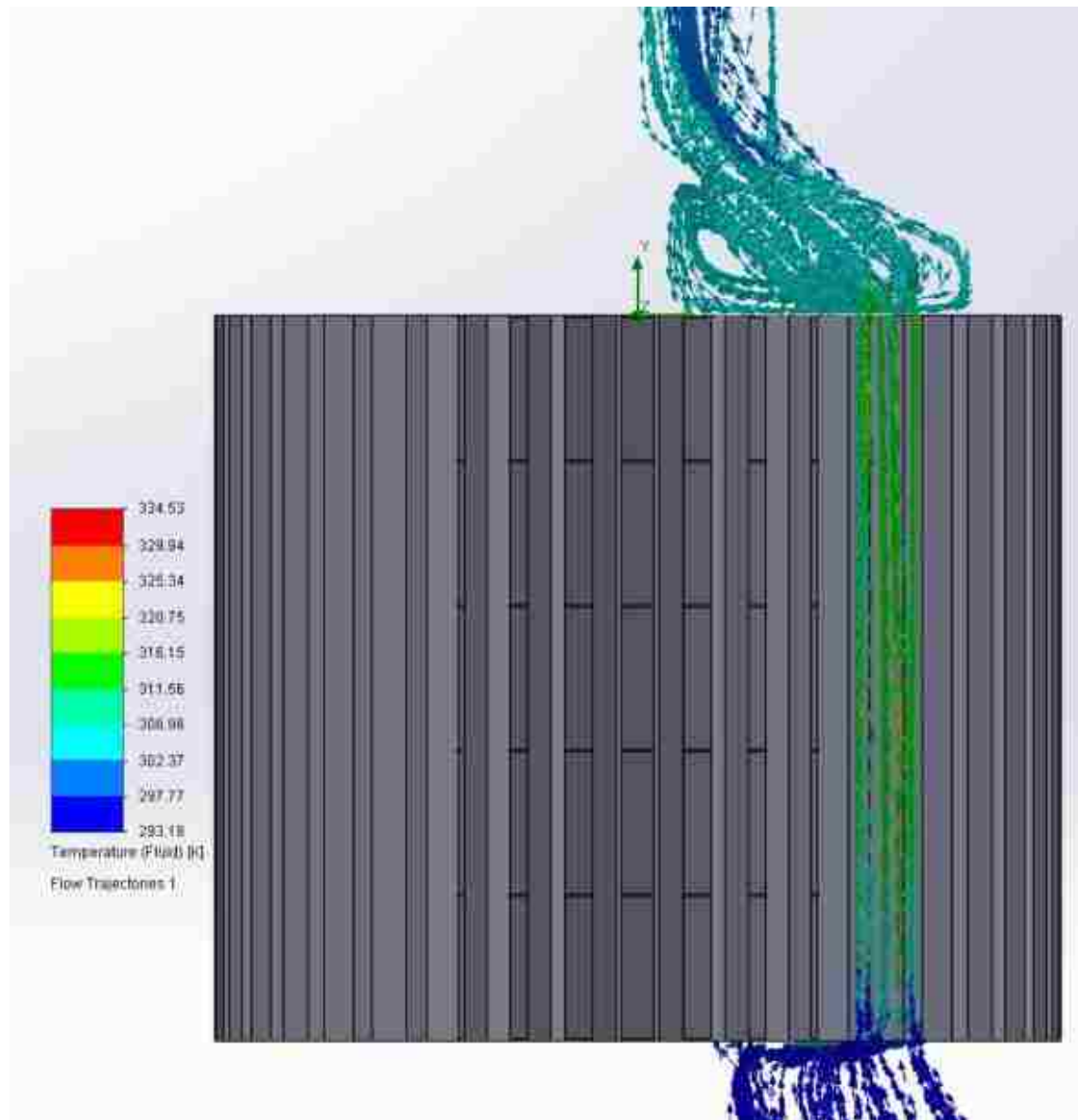


Figure 28: Flow trajectory for configuration 1 between 3 fins only.

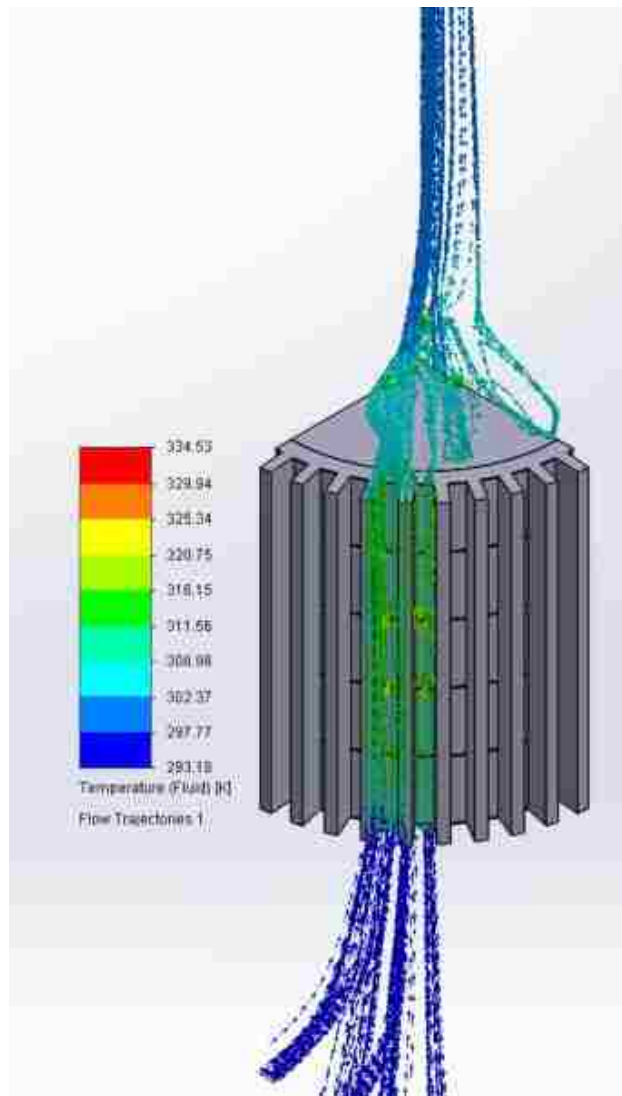


Figure 29: Isometric view of the flow trajectories above.

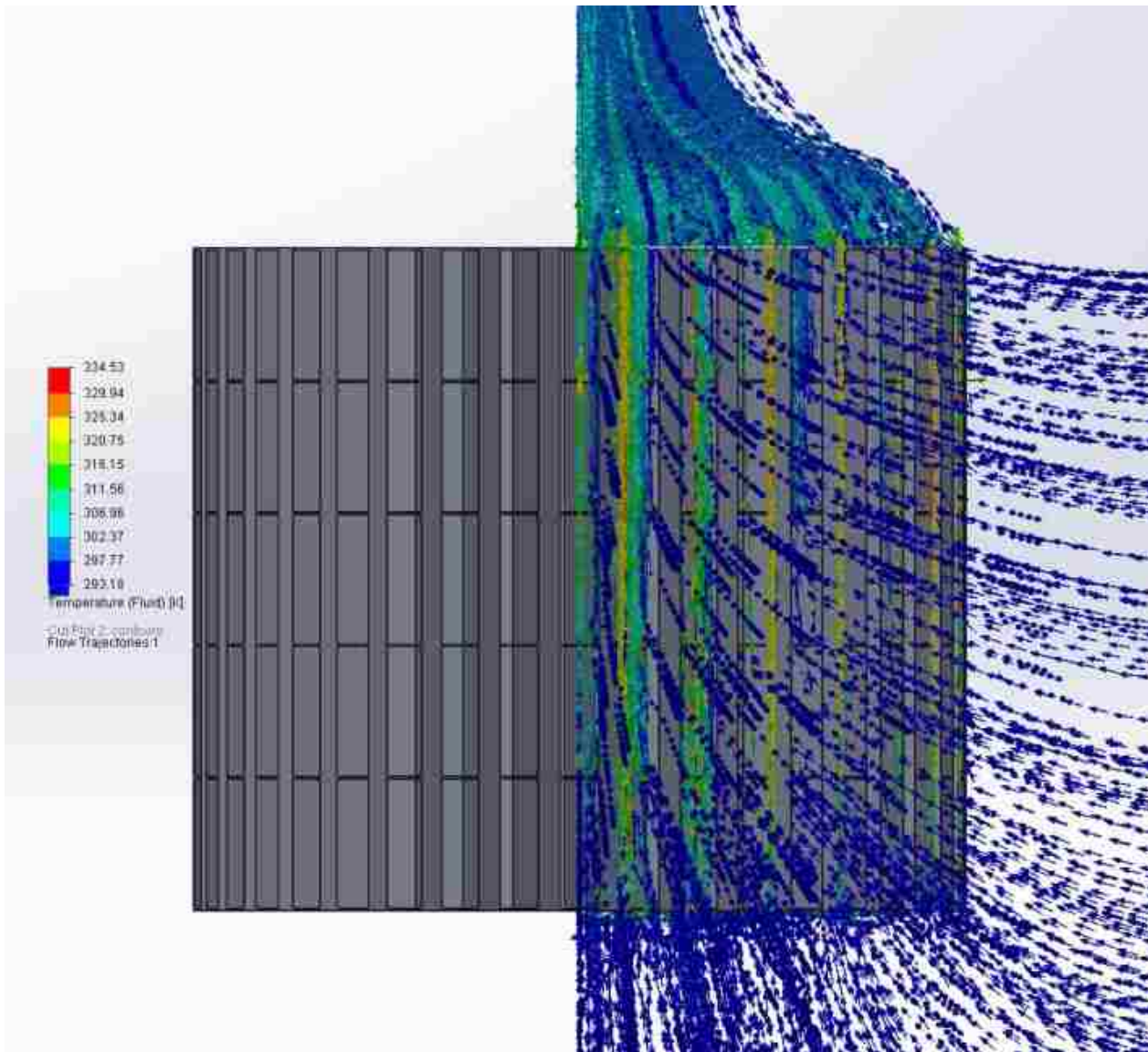


Figure 30: Flow trajectory for configuration 2.

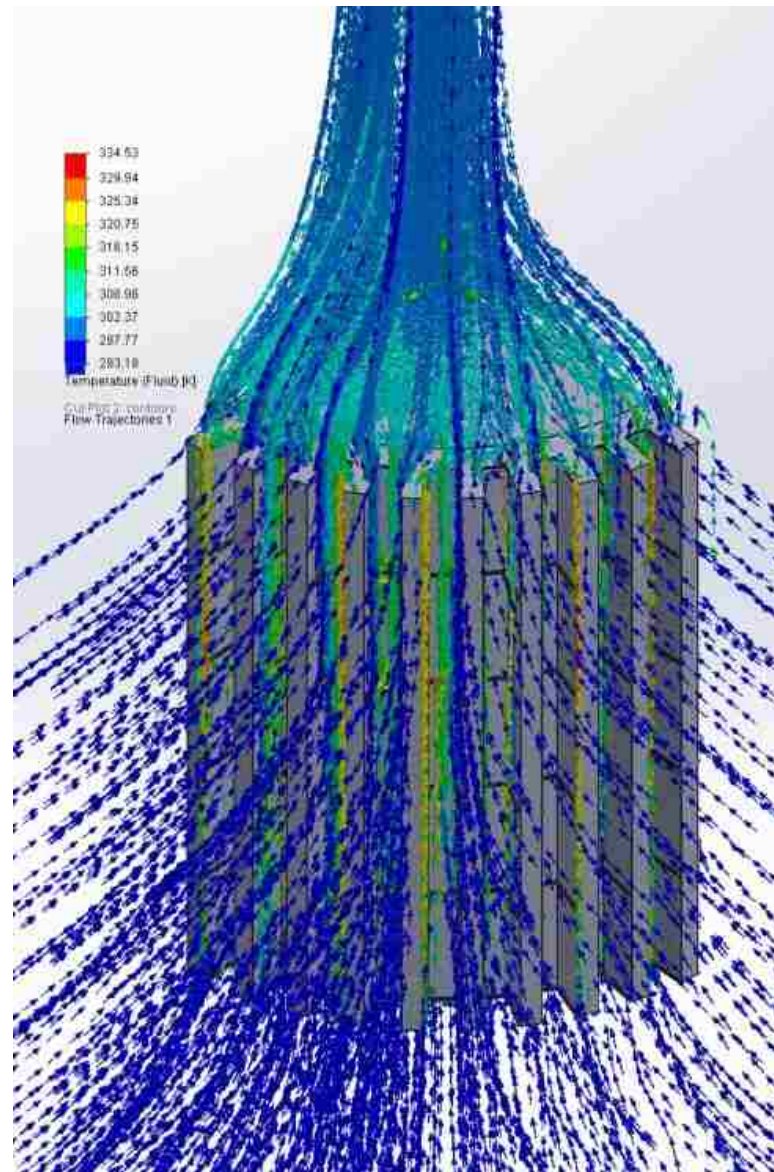


Figure 31: Isometric view of Fig. 30.

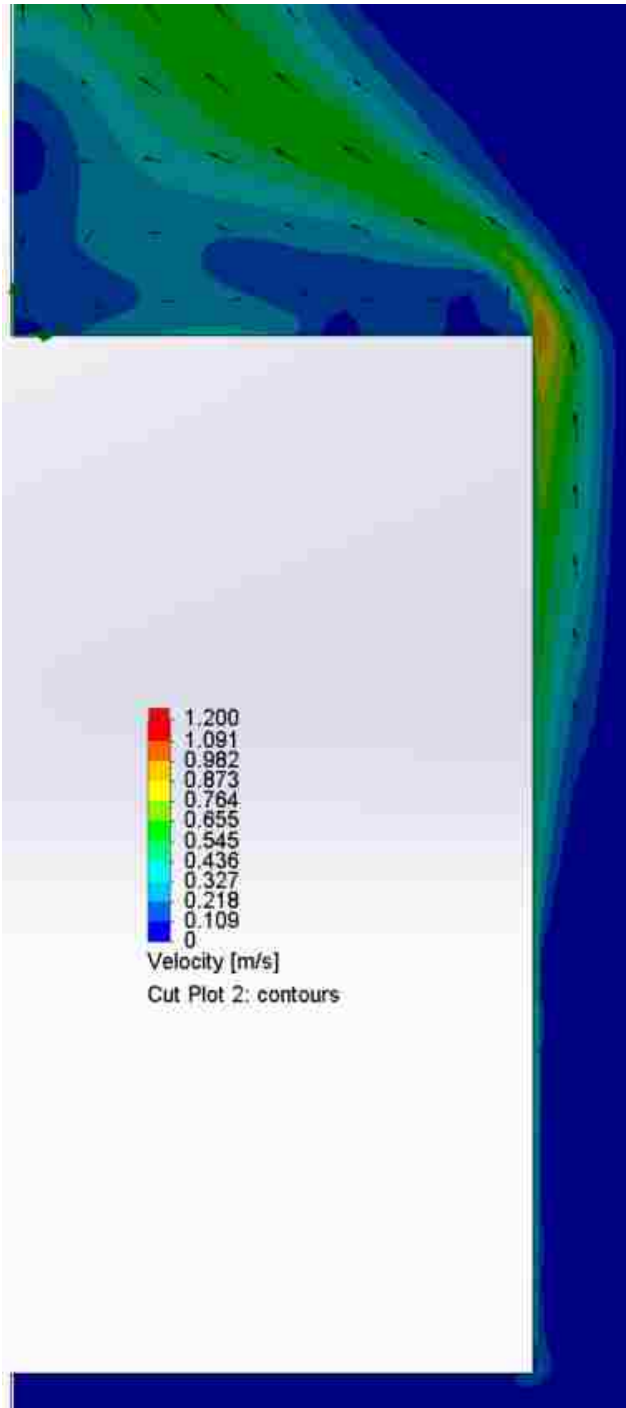


Figure 32: Cut plot showing the fluid velocity for the default configuration.

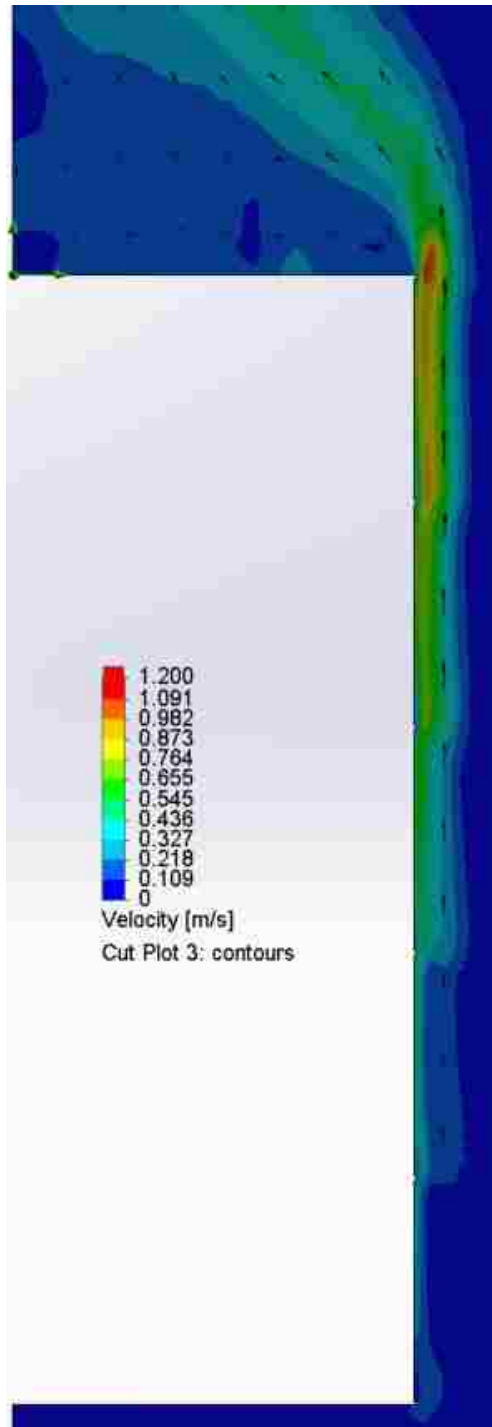


Figure 33: Cut plot showing the fluid velocity for configuration 2.

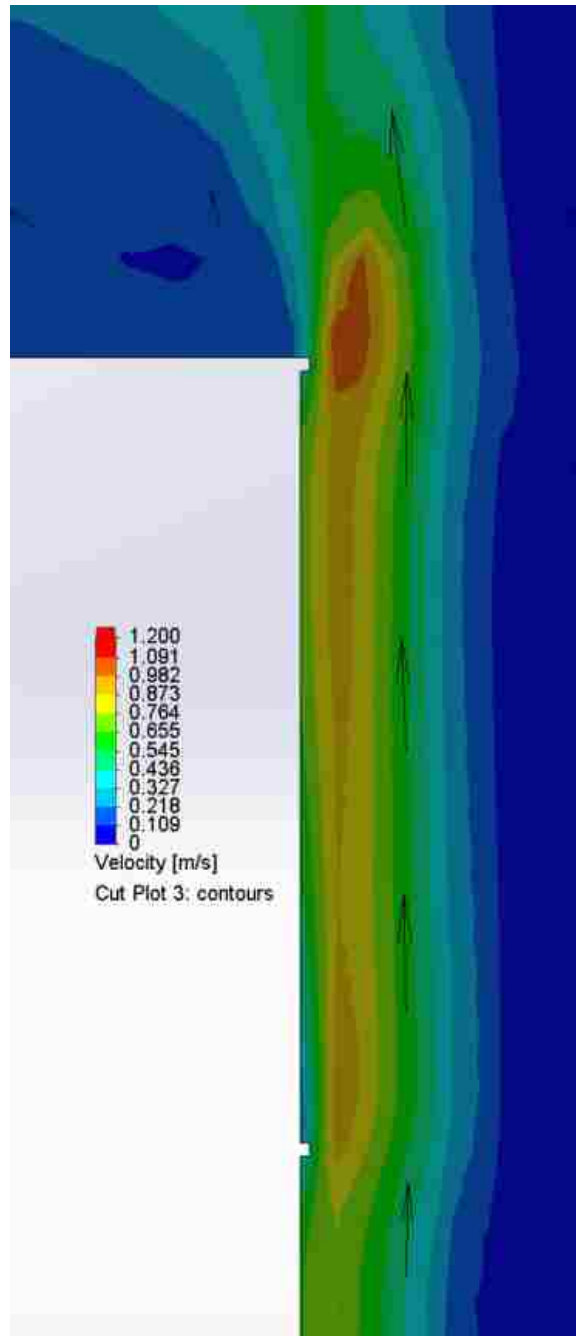


Figure 34: Close up of the fluid velocity at the top edge of the transformer for configuration 2.

A list of the maximum fluid velocities is presented below in Table 2. Note that the average increase in velocity for configuration 1 is 3.24% and 12.87% for configuration 2. Only one data point, configuration 1 with 30 pins, lists a decrease in velocity over the default case which leads to skepticism about the

accuracy of the results. If this data point is ignored, the average increase in velocity for configuration 1 over the default case is 7.15%. Since the convective heat transfer coefficient is directly coupled with flow velocity, these increases will correspond with an increase in heat transfer.

Table 2: Maximum fluid velocities for each configuration.

Maximum Fluid Velocity [m/s]					
# of Fins	Default	Config. 1	% Change	Config. 2	% Change
30	1.520	1.391	-8.48%	1.650	8.53%
40	1.485	1.585	6.73%	1.729	16.39%
50	1.513	1.671	10.49%	1.688	11.62%
60	1.674	1.745	4.23%	1.923	14.92%
		Average Change:	3.24%		12.87%

Figure 35 shown below is a graphical representation of the data presented in Table 2.

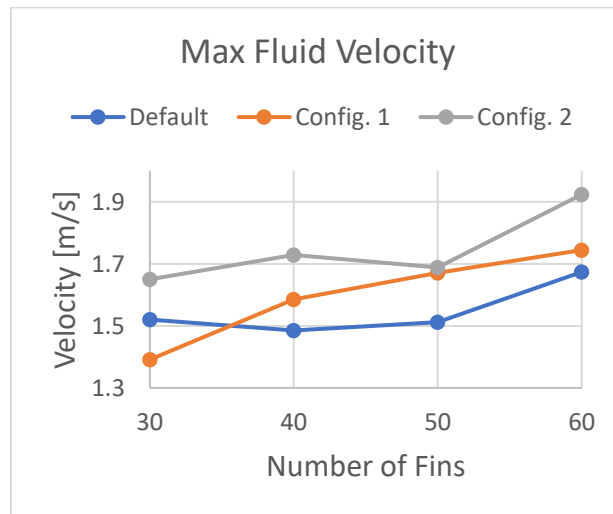


Figure 35: Maximum fluid velocities graphed for each configuration.

5.3 Transformer Temperature Comparison

The maximum temperature of the transformer volume is considered the main goal for the simulations. In the real world, this goal would correspond with the maximum temperature of the internal volume which should be minimized in order to protect electrical components and increase electrical efficiencies. Presented below in Fig. 36, the 3 different geometries are graphed over the number of fins. Table 3 shows the maximum values tabulated, and table 4 shows ΔT , which is the difference in the maximum transformer volume and the inlet temperature of the fluid, 293 K. The overall trend of the temperature is to decrease with number of fins- this makes sense since adding fins increases the surface area of the transformer sleeve, allowing it to dissipate more heat.

Table 3: Maximum transformer temperature for each configuration

Maximum Transformer Temperature [K]					
# of Fins	Default	Config. 1	% Change	Config. 2	% Change
30	332.309	331.618	0.21%	331.569	0.22%
40	327.926	326.819	0.34%	326.103	0.56%
50	323.267	324.532	-0.39%	321.304	0.61%
60	321.298	322.472	-0.37%	319.085	0.69%
		Average Change:	-0.05%		0.52%

Table 4: ΔT for each configuration.

ΔT [K]					
# of Fins	Default	Config. 1	% Change	Config. 2	% Change
30	39.309	38.618	1.76%	38.569	1.88%
40	34.926	33.819	3.17%	33.103	5.22%
50	30.267	31.532	-4.18%	28.304	6.48%
60	28.298	29.472	-4.15%	26.085	7.82%
		Average Change:	-0.85%		5.35%

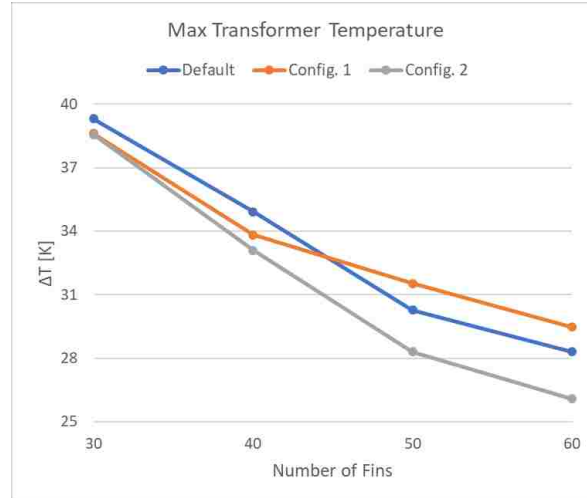


Figure 36: Maximum transformer volume temperature graphed as a function of number of fins for the 3 geometries.

Interestingly, the values for the temperature for the second case, when pins are only added to the base of the sleeve, do not decrease as consistently with number of fins. Temperatures were decreased for the first 2 cases, with a 1.76% improvement with 30 fins, and a 3.17% improvement with 40 fins. However, the temperature for the last 2 cases increased over the default geometry without pins. 50 and 60 fins saw an increase in the maximum temperature of 4.18% and 4.15%, despite the fact that the surface area increased 0.39% from adding pins to the sleeve base. Intuitively, increasing the surface area of the sleeve should transfer more heat, decreasing the maximum temperature of the transformer, but the average change in max temperature actually decreased for configuration 1. Clearly, adding surface area alone does not always increase heat transfer through convection.

Temperature profiles will now be examined. Figure 37 shows a cut plot taken in the channel between the fins of the fluid temperature with velocity represented by arrows. Figures 38-40 show the same cut plot with the solid body hidden for each configuration with 40 fins. Similar to the results for the velocity field, the addition of pins to configurations 1 and 2 disturbs the temperature profile. Pins on the sleeve base only- configuration 1- only slightly changes the temperature profile over the default case

which shows a nice and smooth transition from the bottom of the transformer to the top. In configuration 2, where pins are on the sleeve base as well as the fins, the temperature profile changes dramatically. Regions of high temperature appear behind the pins which correspond to the low-flow regions highlighted in Fig. 34. The profile also gets pushed farther away from the transformer surface, affecting a larger area of fluid. In Fig. 41-43, a zig-zag pattern appears. This is not representative of the isothermal lines, but rather shows the resolution of the mesh at very small distances.

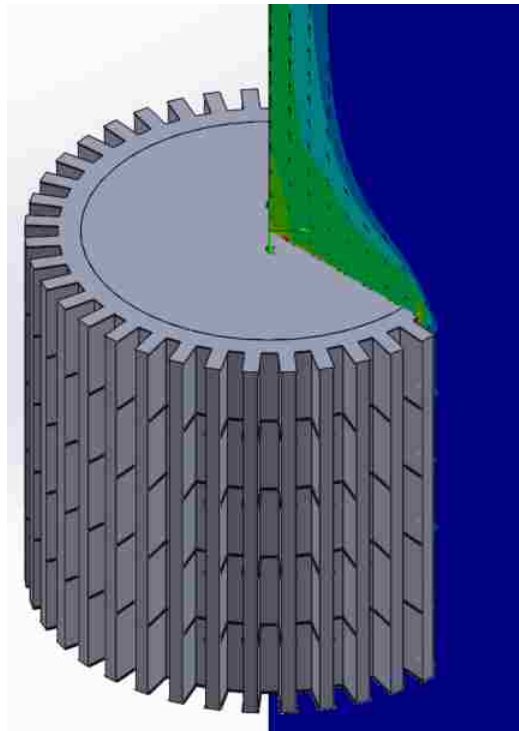


Figure 37: Isometric view of config. 1 shown with a cut plot of fluid temperature between the fins.

Below the temperature cut plots, surface plots of the transformer temperature can be seen in Fig. 44-46. The plots are graphed with the same temperature scales to highlight differences between the 3 configurations. There are notable differences, especially between the default configuration and configuration 2. The addition of the pins to the sleeve base and the fins clearly augments the heat transfer

from the transformer volume. The top and bottom of the fins in Fig. 46 are at or below 323 K, significantly less than the same location in Fig. 44, which shows a temperature around 324.8 K.

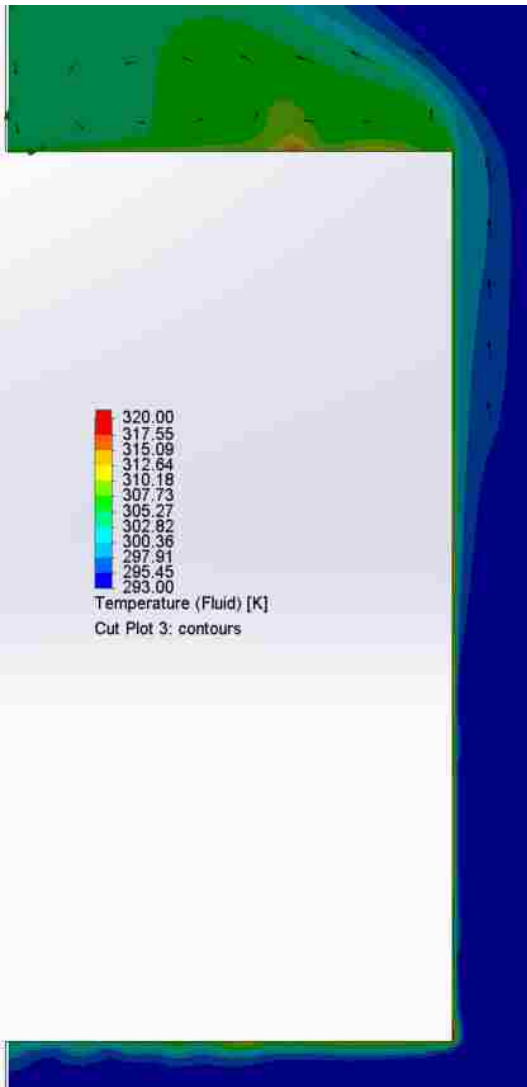


Figure 38: Cut plot of fluid temperature-
default configuration.

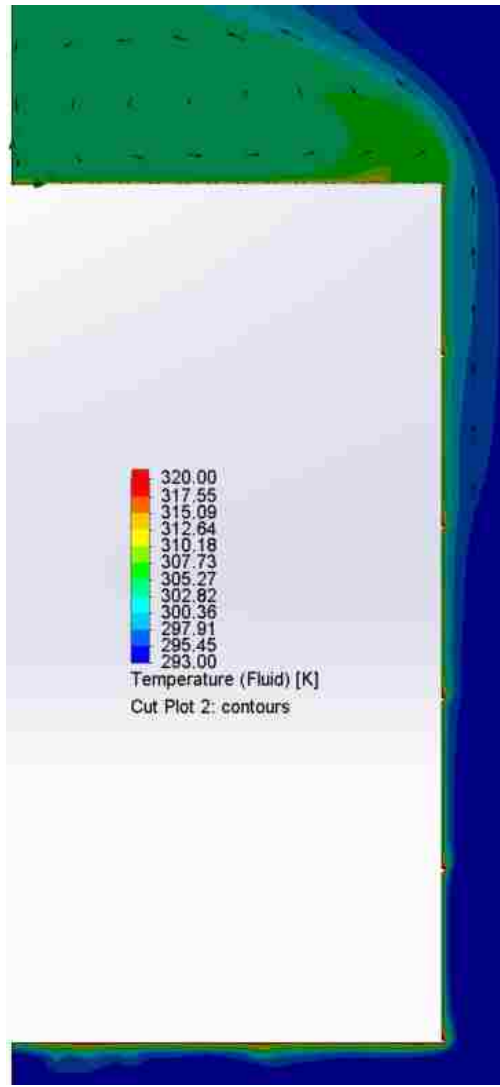


Figure 39: Cut plot of fluid temperature-
configuration 1.

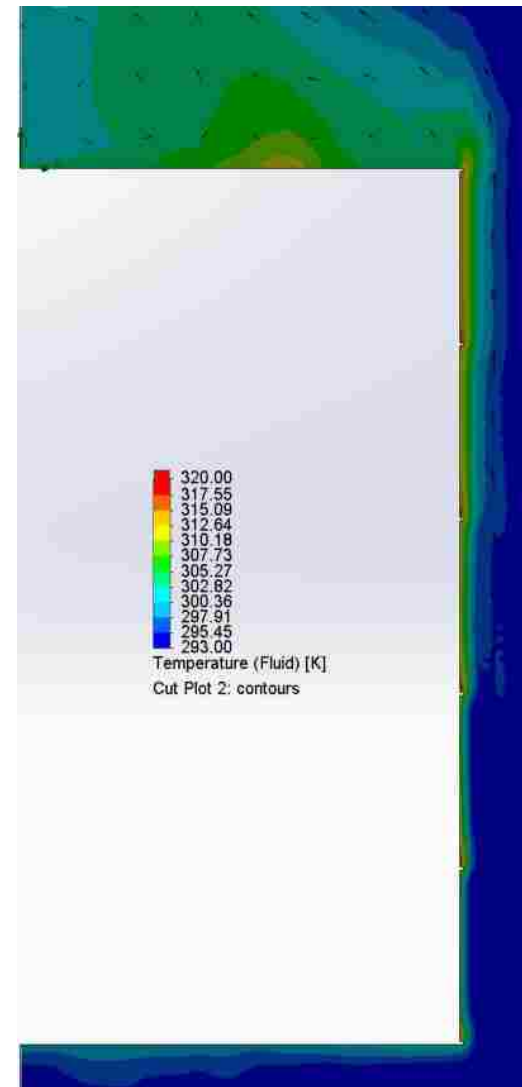


Figure 40: Cut plot of fluid temperature-
configuration 2.

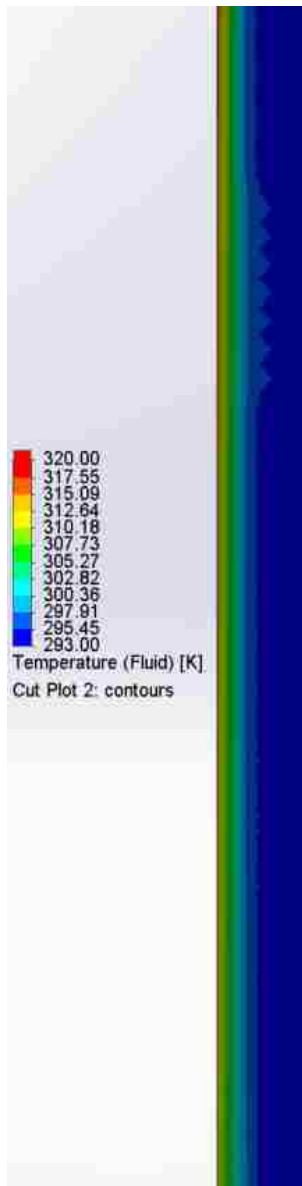


Figure 41: Close up of Fig. 38.

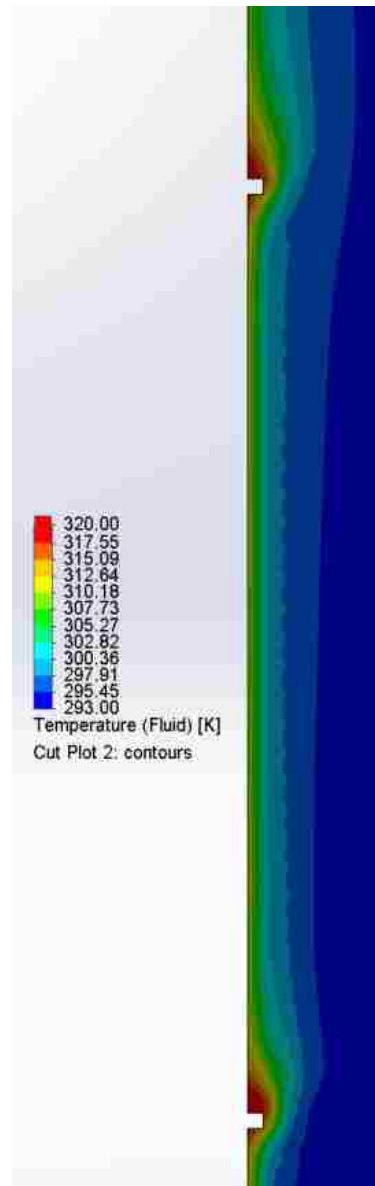


Figure 42: Close up of Fig. 39.

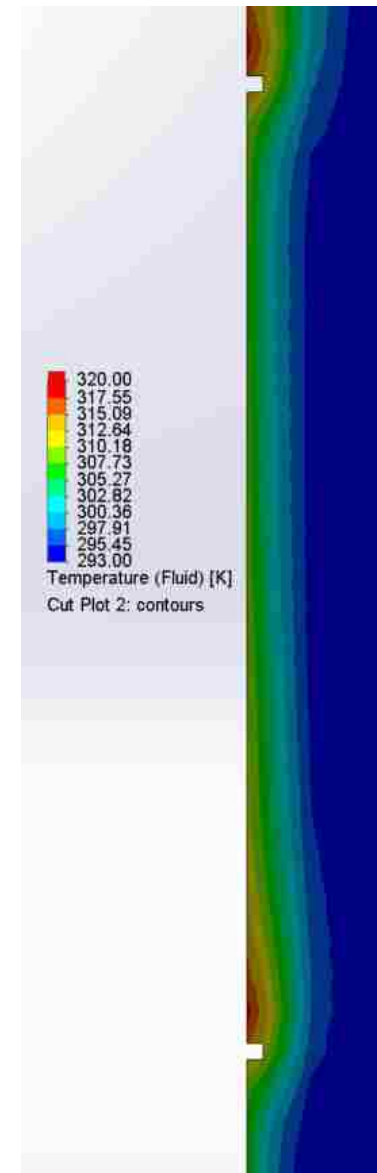


Figure 43: Close up of Fig. 40.

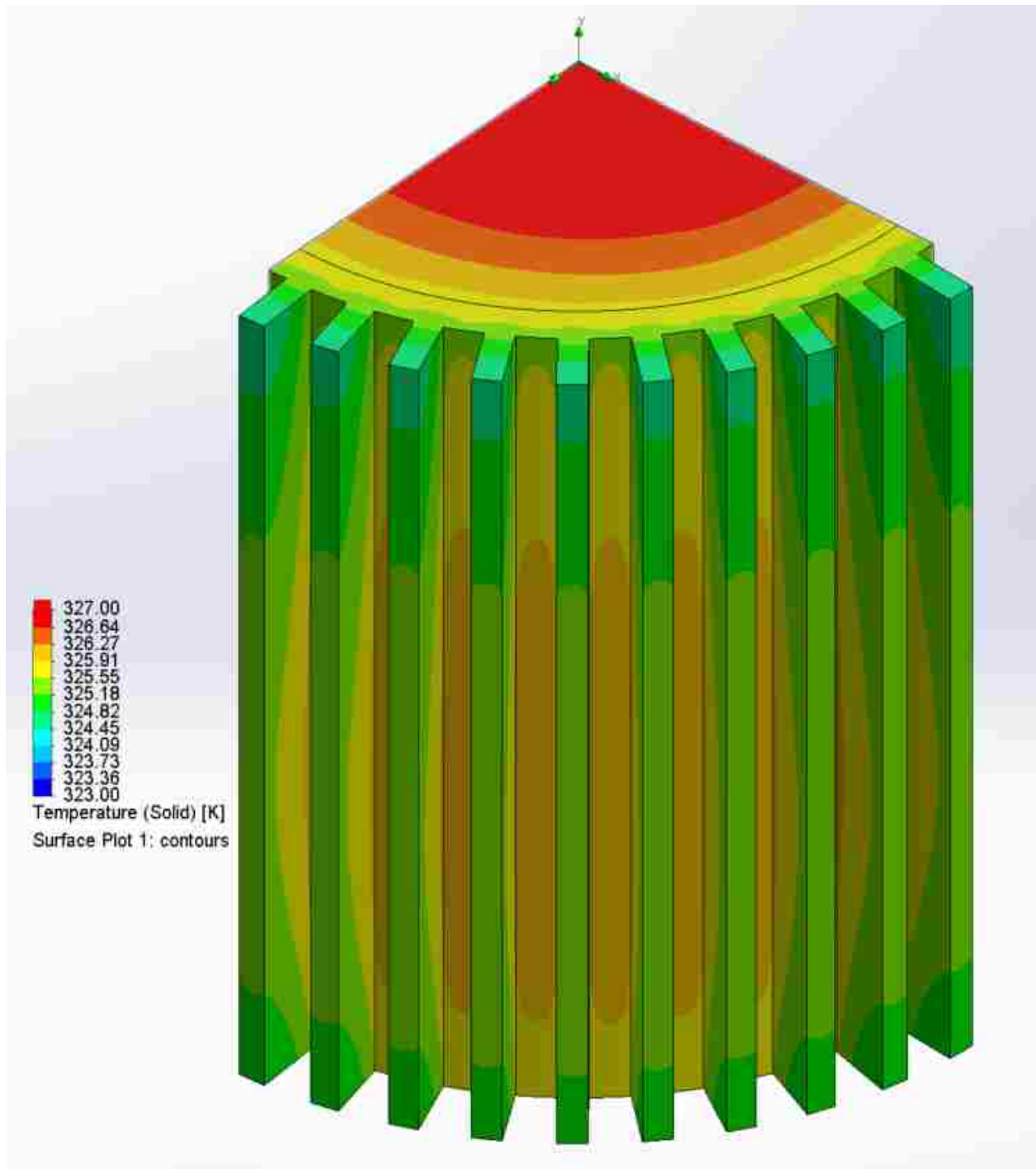


Figure 44: Transformer surface temperature- default configuration.

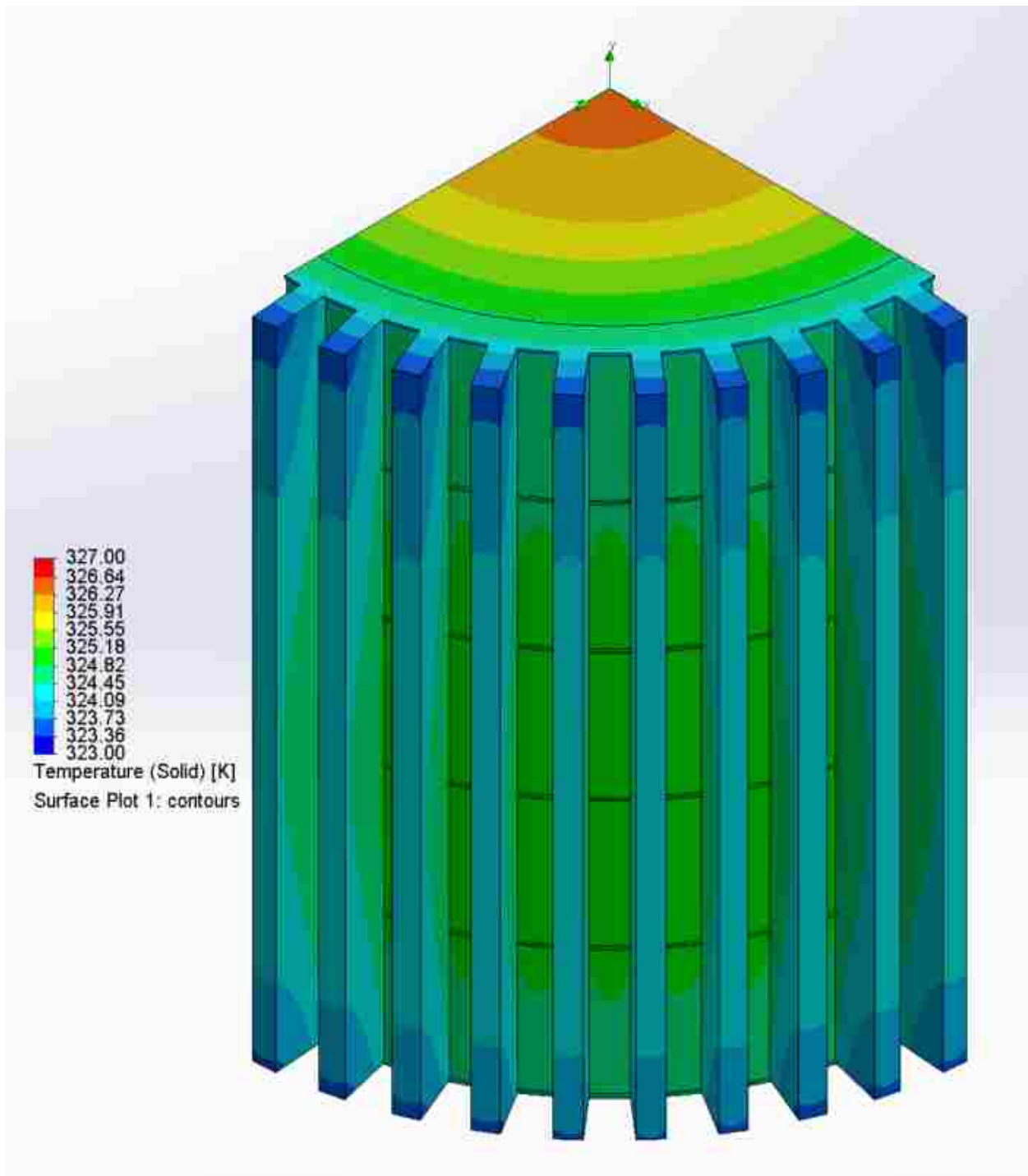


Figure 45: Transformer surface temperature- configuration 1.

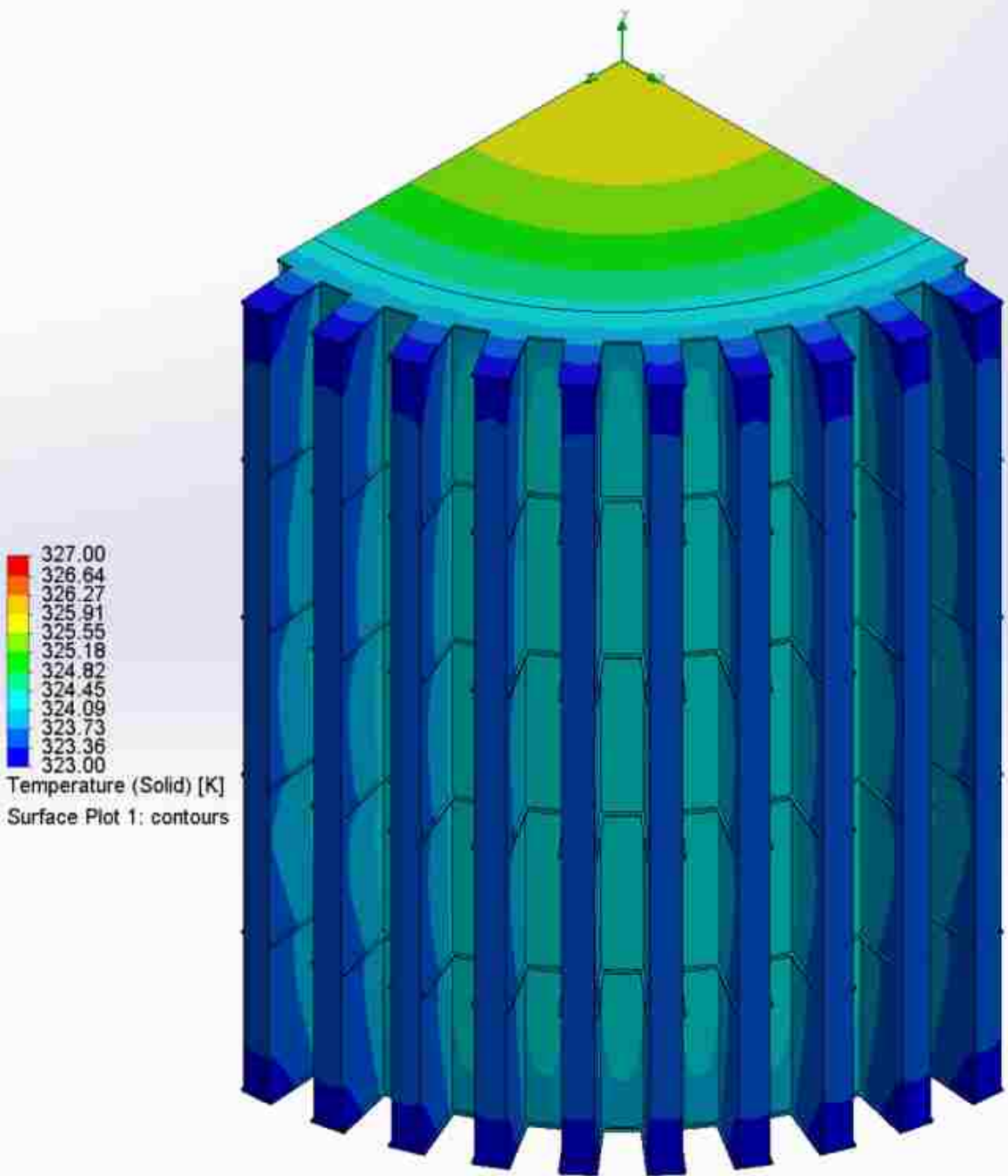


Figure 46: Transformer surface temperature- configuration 2.

5.4 Convective Heat Transfer Coefficient

The convective heat transfer coefficient is to be determined as a function of the number of fins on the transformer sleeve for each of the 3 configurations. The equation for convective heat transfer is given below in Eq. 44:

$$q = hA\Delta T \quad (44)$$

Where q is the heat transfer per unit time, h is the convective heat transfer coefficient, A is the surface area through which the heat transfers, and ΔT is the difference in temperature from the surface to the surrounding fluid. Rearranging Eq. (44) to solve for h gives:

$$h = \frac{q}{A\Delta T}$$

Now q must be determined. From the problem statement, the transformer is generating a heat density of 2500 W/m^3 . In order to convert the volumetric heat density to heat transfer per unit time, the density must be divided by the volume of the cylinder in which it is taking place. The volume of a cylinder is shown below in Eq. (45):

$$V = \pi r^2 H \quad (45)$$

Here H is the height of the cylinder, and r is the radius. q is found by using Eq. (46):

$$q = \frac{q'''}{V} \quad (46)$$

Solving for q :

$$q = \frac{2500 \frac{W}{m^3}}{\pi \left(\frac{2.7}{2} m\right)^2 (3m)} = 42941.6 \text{ W}$$

A, the surface area, is given by SolidWorks and can be seen in Table 5. ΔT was calculated in Table 4 but will be shown again in Table 5. h is also calculated for each configuration and can be found at the bottom of Table 5.

Table 5: Convective heat transfer coefficient calculated for each configuration.

	Default	Config. 1	Config. 2
# Fins	A [m²]		
30	139.80	140.61	142.27
40	155.30	155.91	158.22
50	170.80	171.28	174.16
60	186.30	186.64	190.10
	ΔT [°C]		
30	39.3088	38.6183	38.5692
40	34.9256	33.8189	33.1028
50	30.2669	31.5320	28.3043
60	28.2976	29.4717	26.0852
	h [W/m²-°C]		
30	7.8141	7.9080	7.8257
40	7.9170	8.1441	8.1988
50	8.3066	7.9510	8.7112
60	8.1455	7.8067	8.6597

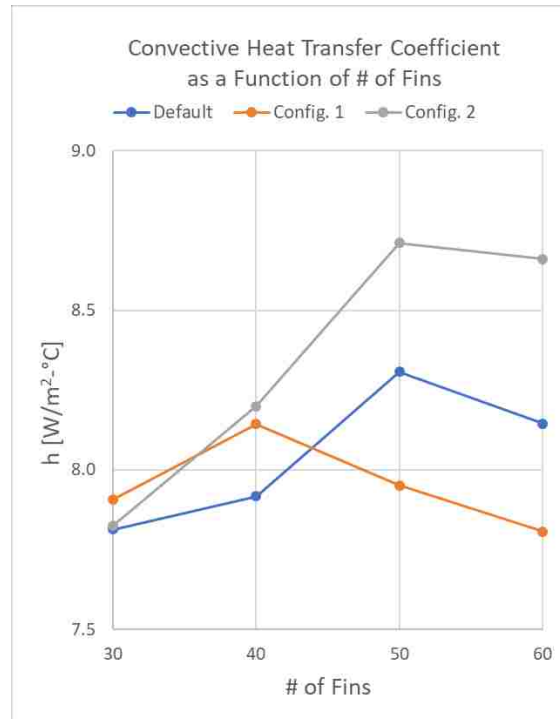


Figure 47: Graphical representation of the convective heat transfer coefficient per # of fins.

Figure 47 graphs the results of h over the range of fins for each configuration. Interestingly, the value for h decreases for 60 fins versus 50 fins. Since the surface area increases with the addition of more fins, intuitively the heat transfer should increase. It appears that the upper limit of number of fins for these configurations to maximize heat transfer have been found. The peaks in the graph, 50 fins for the default and config. 2, and 40 fins for config. 1, represent the maximum heat transfer with these specific geometries. Figures 48-49 below shows the difference between 50 fins and 60 fins for configuration 2.

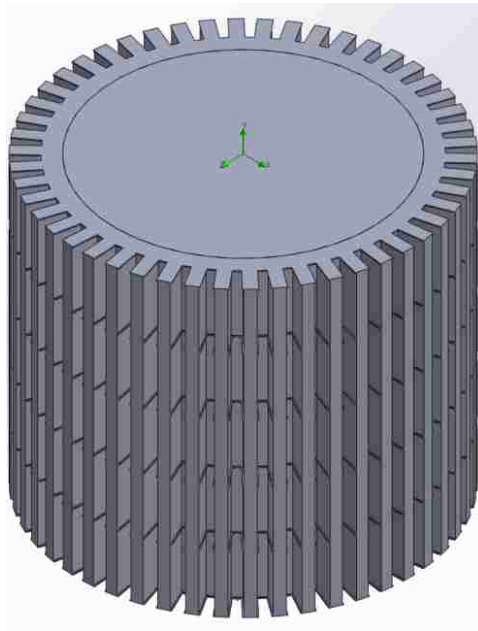


Figure 48: Configuration 2 with 50 fins.

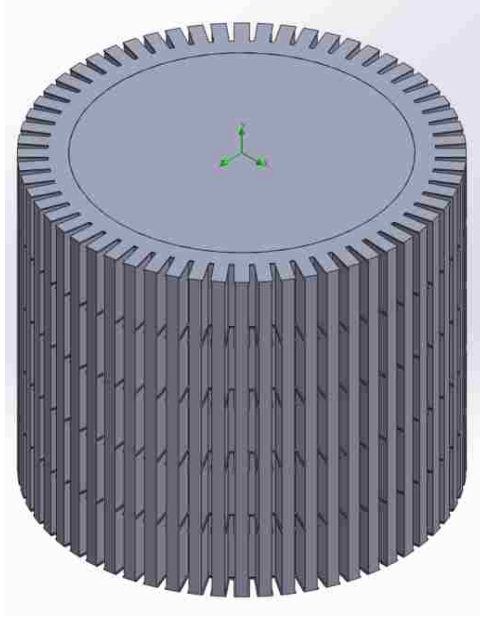


Figure 49: Configuration 2 with 60 fins.

The channel between the fins is where most of the natural convection will occur. When it becomes too small, there will not be enough fluid area that will be exposed to the fin and pin area. Such is the case in Fig. 49- the channel width is too small to maximize the heat transfer between fluid and solid surfaces. Even though the surface area is increased overall, the convection is limited. Comparing cut plots of the fluid temperature for configuration 2 for 50 and 60 fins, shown in Fig. 50-51, there are no obvious answers for why h decreases between those 2 cases.

One area that might provide insight is the green wake at the top of the transformer. This area is enlarged in Fig. 52-53. In Fig. 52, the wake is more solid and continues to the top edge of the image. Alternatively, the wake in Fig. 53 is much smaller and quickly dissipates. This shows that there is less fluid volume at the high temperature at the top edge of the transformer which causes the wake to be more subject to the surrounding fluid temperature.

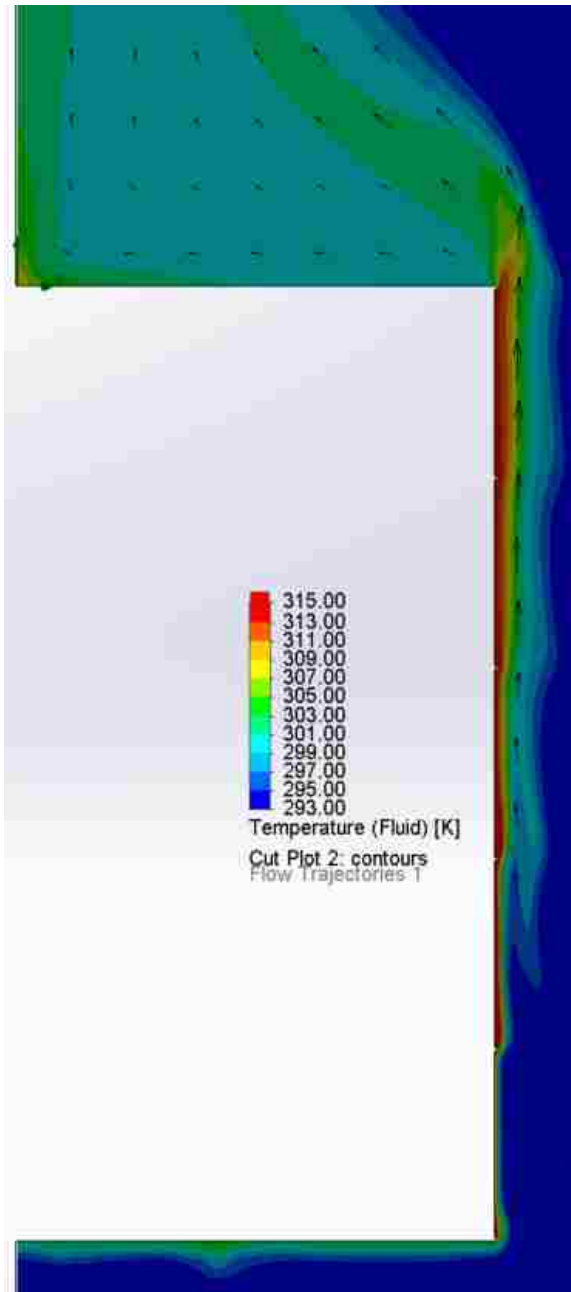


Figure 50: Cut plot of fluid temperature for configuration 2 with 50 fins.

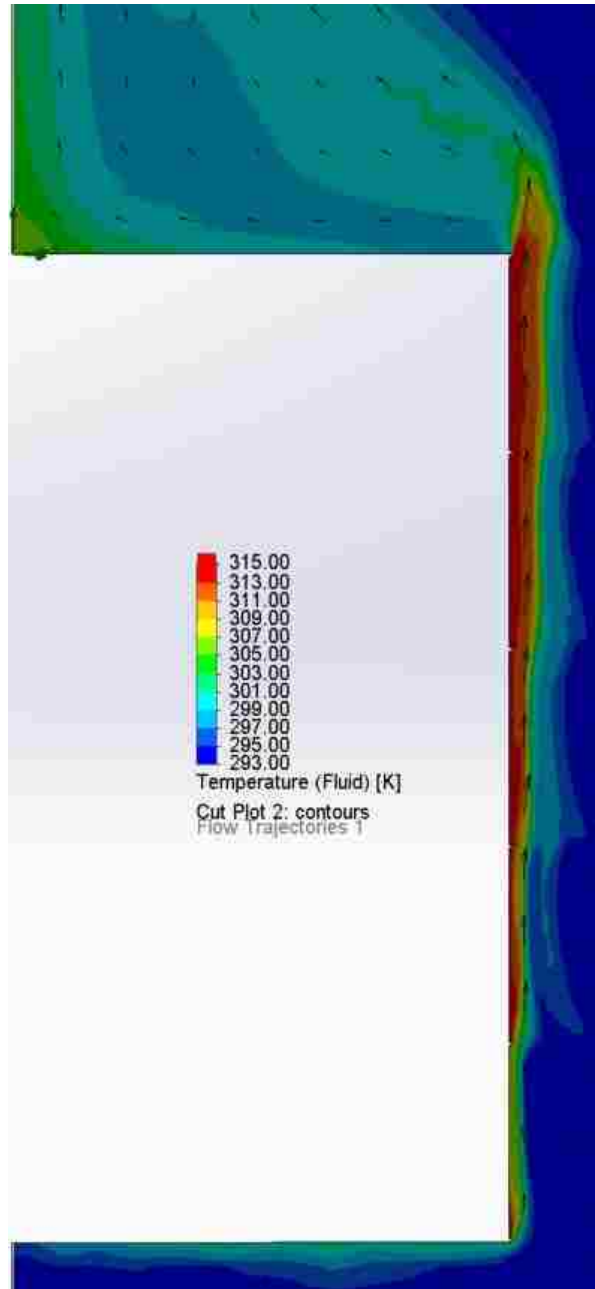


Figure 51: Cut plot of fluid temperature for configuration 2 with 60 fins.

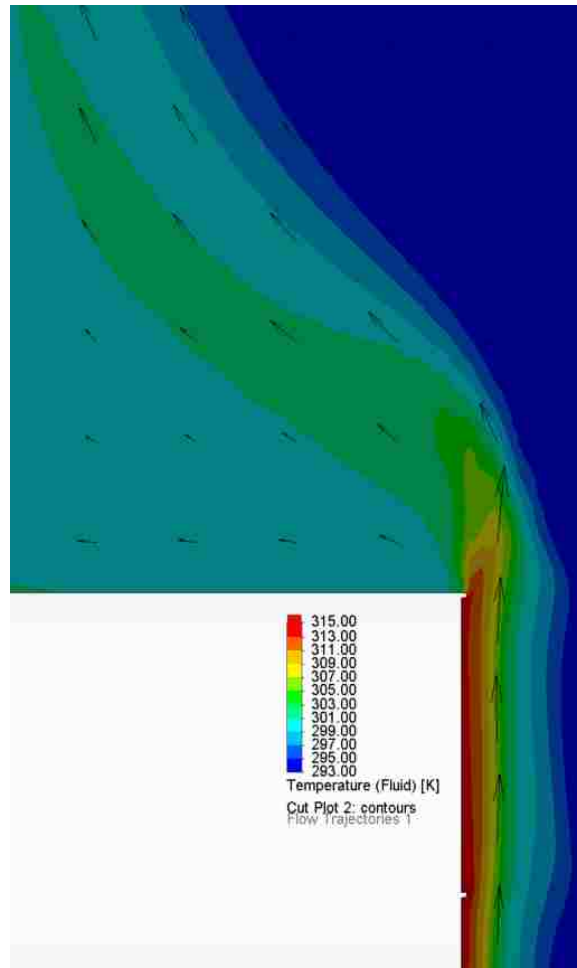


Figure 52: Close up of the wake at the top edge of the transformer from Fig. 50.

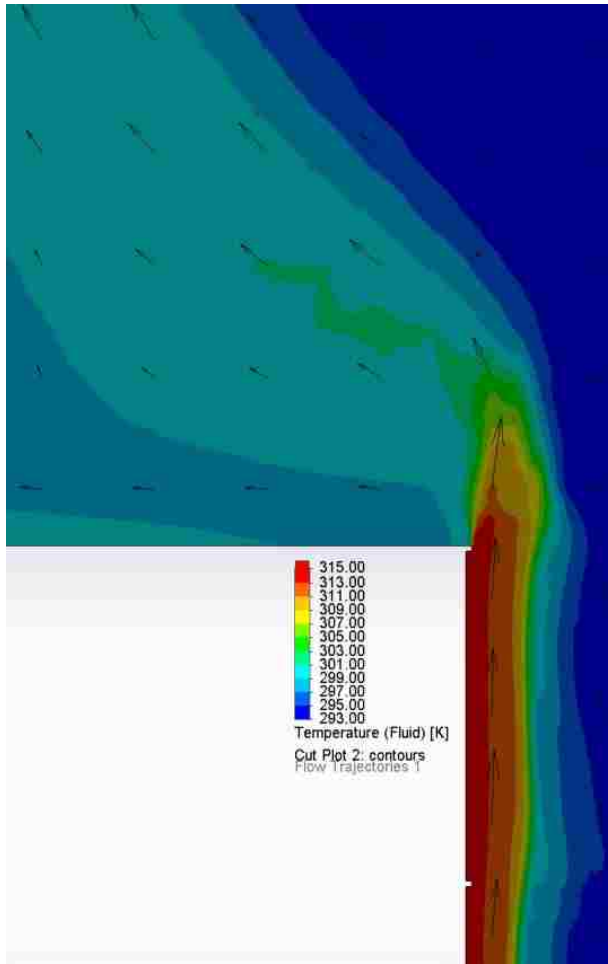


Figure 53: Close up of the wake at the top edge of the transformer from Fig. 51.

6. Conclusion

In general, adding surface area through the use of fins is an effective way to augment heat transfer through convection. When the space between the fins becomes too small, the heat transfer may be limited since the amount of fluid that can enter the channel is reduced. This was shown to be the case in Fig. 47. The graph showing the natural convective heat transfer coefficient has clear peaks for each configuration, confirming that there are ideal geometries and numbers of fins to optimize heat transfer.

The addition of pins to the sleeve body only produced conflicting results. Since the surface area of the sleeve increased with the addition of the pins, the heat flux through the sleeve should have been increased. Configuration 1 with 30 and 40 fins did see a decrease in the maximum volume temperature of the transformer, but the trend did not continue. Between 40 and 50 fins, the graph crossed over the default configuration and actually increased the transformer temperature. Future studies could be performed to find the exact number of fins at which this cross over takes place.

Configuration 2, placing pins on the sleeve base as well as on the fins, proved to be an effective way to exploit the natural convection between the fin channels. There were substantial increases in the heat transfer coefficient for all numbers of fins, an average of a 3.7% increase over the default configuration. The addition of the pins disturbed the flow between the fins which caused more of the surrounding fluid to be exposed to the transformer surface. The fluid and thermal boundary layers were also disturbed, minimizing the effects these have on reducing heat transfer. Future work could look into changing the shape of these pins to study the effect of shape on heat transfer and could also vary the number of horizontal pins that are placed along the transformer sleeve. Like with the number of fins, there is a number at which horizontal pins will actually increase the maximum temperature of the transformer.

This paper has been an in-depth look into SolidWorks Flow Simulation and has provided insight into the inner-workings of the program. Having this knowledge will aide in future simulation work, saving time in the setup, meshing, and solving of 3D fluidic systems.

References

- [1] Shaukatullah, H., Storr, W., Hansen, B. and Gaynes, M., 1996, "Design and optimization of pin fin heat sinks for low velocity applications," IEEE Transactions on Components, Packaging, and Manufacturing Technology: Part A, **19**(4), pp.486-494.
- [2] Bruns, T., 2007, "Topology optimization of convection-dominated, steady-state heat transfer problems," International Journal of Heat and Mass Transfer, **50**(15-16), pp.2859-2873.
- [3] Li, Q., Steven, G., Xie, Y. and Querin, O., 2004, "Evolutionary topology optimization for temperature reduction of heat conducting fields," International Journal of Heat and Mass Transfer, **47**(23), pp.5071-5083.
- [4] Klaas Haertel, J. H., Engelbrecht, K., Lazarov, B. S., & Sigmund, O., 2015, "Topology Optimization of Thermal Heat Sinks," In Proceedings, COMSOL conference 2015.
- [5] Sigmund, O., 2001, "A 99 line topology optimization code written in Matlab," Structural and Multidisciplinary Optimization, **21**(2), pp.120-127.
- [6] Morrone, B., Campo, A. and Manca, O. (1997). Optimum plate separation in vertical parallel plate channels for natural convective flows: incorporation of large spaces at the channel extremes. International Journal of Heat and Mass Transfer, **40**(5), pp.993-1000.
- [7] Baskaya, S. and Kanli, H. (2004). Effects of plate separation, plate length and temperature difference on buoyancy driven heat transfer in finite horizontal parallel plates. Heat and Mass Transfer, **40**(3-4), pp.293-300.
- [8] Radziemska, E. and Lewandowski, W. (2005). Free Convective Heat Transfer Structures as a Function of the Width of Isothermal Horizontal Rectangular Plates. Heat Transfer Engineering, **26**(4), pp.042-050.
- [9] Khalifa, A., 2000, "Natural convective heat transfer coefficient – a review II. Surface in two- and three-dimensional enclosures," Energy Conversion and Management, **42**(2001), pp.505-517.
- [10] Desrayaud, G. and Fichera, A., 2002, "Laminar natural convection in a vertical isothermal channel with symmetric surface-mounted rectangular ribs," International Journal of Heat and Fluid Flow, **23**(4), pp.519-529.
- [11] Wang, X. and Pepper, D., 2009, "Numerical simulation for natural convection in vertical channels," International Journal of Heat and Mass Transfer, **52**(17-18), pp.4095-4102.
- [12] Cruchaga, M. and Celentano, D., 2003, "Modelling natural and mixed convection in obstructed channels," International Journal of Numerical Methods for Heat & Fluid Flow, **13**(1), pp.57-85.
- [13] Kozanoglu, B. and Lopez, J., 2006, "Thermal boundary layer and the characteristic length on natural convection over a horizontal plate, Heat and Mass Transfer, **43**(4), pp.333-339.
- [14] Lee, S., 1997, "Optimum design and selection of heat sinks," Microelectronics Reliability, **37**(4), pp.699.

- [15] Dede, E., Joshi, S. and Zhou, F., 2015, "Topology Optimization, Additive Layer Manufacturing, and Experimental Testing of an Air-Cooled Heat Sink," *Journal of Mechanical Design*, **137**(11), pp.111403.
- [16] Sakanova, A. and Jet Tseng, K., 2018, "Comparison of pin-fin and finned shape heat sink for power electronics in future aircraft," *Applied Thermal Engineering*.
- [17] Dassault Systemes, 2014, "Numerical Basis of CAD-Embedded CFD White Paper," [online] Available at: <https://www.solidworks.com/sw/numerical-basis-cad-embedded-cfd-confirmation.htm>
- [18] Lam, C. and Bremhorst, K., 1981, "A Modified Form of the k- ϵ Model for Predicting Wall Turbulence," *Journal of Fluids Engineering*, **103**(3), p.456.
- [19] Balakin, V., Churbanov, A., Gavriliouk, V., Makarov, M. and Pavlov A., 2004, "Verification and Validation of EFD.Lab Code for Predicting Heat and Fluid Flow," *Proceedings of ICHMT International Symposium on Advances in Computational Heat Transfer, Norway, April 19-24, 2004*.
- [20] Ginzburg, I.P., 1970, "Theory of Drag and Heat Transfer," Leningrad, LGU (in Russian).
- [21] Van Driest, E.R., 1956, "On Turbulent Flow Near a Wall," *Journal of the Aeronautical Science*, **23**(10), pp. 1007-1011.

Curriculum Vitae

Sean Ferneyhough, M.S.E.

Email: ferneyhough.sean@gmail.com

Education

University of Nevada, Las Vegas

MSE, Mechanical Engineering, May 2018

Graduate Assistant, course instructor EGG 100, ME 240

University of Nevada, Reno

BS, Mechanical Engineering, May 2015